Coherent Control of Quantum Dynamics with Sequences of Unitary Phase-Kick Pulses

Luis G.C. Rego,[1] Lea F. Santos,[2] and Victor S. Batista[3]

[1]Departamento de Física, Universidade Federal de Santa Catarina, Florianópolis, SC 88040-900 Brazil; email: lrego@fisica.ufsc.br

[2]Department of Physics, Yeshiva University, New York, New York 10016; email: lsantos2@yu.edu

[3]Department of Chemistry, Yale University, New Haven, Connecticut 06520-8107; email: victor.batista@yale.edu

Annu. Rev. Phys. Chem. 2009. 60:293–320

First published online as a Review in Advance on November 21, 2008

The *Annual Review of Physical Chemistry* is online at physchem.annualreviews.org

This article's doi: 10.1146/annurev.physchem.040808.090409

0066-426X/09/0505-0293$20.00

Key Words

dynamical decoupling, quantum information, NMR, tunneling, bang-bang, decoherence, quantum dots, TiO_2

Abstract

Coherent-optical-control schemes exploit the coherence of laser pulses to change the phases of interfering dynamical pathways and manipulate dynamical processes. These active control methods are closely related to dynamical decoupling techniques, popularized in the field of quantum information. Inspired by nuclear magnetic resonance spectroscopy, dynamical decoupling methods apply sequences of unitary operations to modify the interference phenomena responsible for the system dynamics thus also belonging to the general class of coherent-control techniques. This article reviews related developments in the fields of coherent optical control and dynamical decoupling, emphasizing the control of tunneling and decoherence in general model systems. Considering recent experimental breakthroughs in the demonstration of active control of a variety of systems, we anticipate that the reviewed coherent-control scenarios and dynamical-decoupling methods should raise significant experimental interest.

1. INTRODUCTION

Tunneling: classically forbidden penetration through a potential energy barrier

Nuclear magnetic resonance (NMR): spectroscopic technique that probes the structural and magnetic properties of atomic and molecular systems

RF: radiofrequency

The development of practical methods for controlling quantum dynamics with electromagnetic fields has a long history and remains an outstanding challenge of great technological interest (1–6). This review focuses on coherent-control scenarios based on sequences of unitary pulses that can significantly influence quantum dynamics (e.g., suppress, or accelerate, quantum tunneling). The pulses achieve control by changing the relative phases of interference dynamical pathways in coherent superposition states, without modifying the potential energy surfaces responsible for reaction dynamics (7, 8), or collapsing the coherent unitary evolution of the system as in control schemes based on the quantum Zeno effect (9–13). The reviewed coherent-control methods are also fundamentally different from traditional kinetic control methods in which experimental conditions (e.g., the effect of temperature, pressure, catalysts, or external potentials) are controlled to favor (or suppress) dynamical pathways. The coherent-control sequences discussed here could be optimized by using closed-loop techniques that monitor the outcome of the control process to improve the control sequence and achieve the desired dynamics (14, 15). The discussion of such optimization methods, however, is beyond the scope of our presentation.

Quantum coherent-control methods based on sequences of externally applied electromagnetic-field pulses have long been considered in nuclear magnetic resonance (NMR) spectroscopy. Indeed, the earliest experimental implementations of quantum coherent control (demonstrating active control over the coherent dynamics of molecular systems) date from the 1950s. These experiments aimed at eliminating the undesired phase evolution by applying trains of radiofrequency (RF) π pulses, the so-called spin-echo effect and Carr-Purcell sequences (16, 17). During the ensuing decades, the technique led to a multitude of RF pulse sequences that were extensively used to study molecular structure and dynamics (18–20). A prototype example is the WAHUHA sequence for the suppression of dipolar interactions via sequences of $\pi/2$ pulses (21).

In 1957, the demonstration that all two-level systems are mathematically equivalent suggested that coherent light pulses could lead to optical-quantum-control methods analogous to NMR techniques (22). Not surprisingly, the development of the first high-power lasers in the 1960s was rapidly followed by the demonstration of the photon-echo effect (23). However, methods to control events at the molecular scale with laser pulses were proposed only in the 1980s and bore little resemblance to NMR techniques (14, 24–28). Instead of using sequences of pulses to perturb the quantum evolution of the systems along the course of the dynamical processes, the early coherent-optical-control methods typically prepared the system in an initial coherent superposition by using multiple (or tailored) laser pulses. The system then evolved freely, and the components of the initial coherent superposition interfered with each other while following competing relaxation pathways. Therefore, coherent-optical-control methods have focused mainly on the rational design, preparation, and optimization of initial coherent superposition states (15, 29–40). Nowadays, ultrafast lasers can produce a wide range of complex pulses with ultrashort time resolution and extremely high-peak powers (41–44). As a result, a variety of coherent-control methods based on sequences of ultrafast laser pulses have been proposed (41–44), including the suppression of quantum tunneling by affecting the relative phases of interfering dynamical pathways (4–6). The ultimate goal of these developments has been to provide fundamental understanding on how to manipulate quantum mechanical interferences to control the dynamics of quantum systems ranging from single atoms and molecules to Josephson junction–based devices and nanomechanical resonators.

Quantum coherences that are essential for coherent-control techniques can be preserved even in rather complex systems, as observed by photon-echo (45), pump-probe (46), and fluorescence upconversion experiments (47) for the vibrational quantum beats of electronic states of organic dyes in liquids and condensed phases. Moreover, engineered solid-state devices at the nano- and

microscales provide a rich ground for the observation of coherent quantum tunneling effects. Particularly, coherent charge oscillations have been produced in double–quantum dot (QD) systems (48, 49) and Cooper-pair boxes (i.e., nanometer-scale superconducting electrodes connected to a reservoir via a Josephson junction) (50). Furthermore, in atomic physics, coherent quantum dynamics has been studied in ions and atomic Bose-Einstein condensates confined by optical traps (51). However, in most systems, decoherence is the main obstacle hindering the achievement of coherent control.

Decoherence is a ubiquitous phenomenon in quantum systems, caused by the interactions with the environment. One of its consequences is the randomization of quantum phases associated with coherent superposition states, making quantum-control techniques ineffective. The decoherence timescales range from femtoseconds to nanoseconds for electronic excitations, owing to coupling with phonons and spontaneous emission, whereas spin-coherent excitations decohere in microseconds to milliseconds owing to coupling to other spins in the sample or spin-orbit interaction. Several strategies have been proposed for suppressing decoherence, including quantum error-correction schemes (52, 53) and decoherence-free subspaces (54). Here, we focus on dynamical-decoupling techniques (55–58) that actively decouple the system of interest from its environment by using control pulse sequences inspired by NMR spectroscopy. The first theoretical description of the dynamical-decoupling method considered a sequence of spin echoes applied to a single spin-1/2 with the purpose of suppressing its interaction with a bosonic reservoir (56). The method was termed quantum bang-bang control, after its classical analog (59–61), referring to the ideal situation of arbitrarily strong and instantaneous pulses. The so-called hard pulses in NMR are analogous to this picture. Soon afterward, dynamical-decoupling schemes were incorporated into a theoretical framework in which the control operations are drawn from a discrete control group (55, 57, 58).

Quantum-control methods based on dynamical decoupling have been studied in connection to a wide range of applications, including the suppression of internal and external interactions as well as the control of transport behavior (62), and have become particularly popular in the area of quantum information (63, 64). Among the various contributions to the development of dynamical-decoupling methods, we mention the following (for a more complete list of references, see 65, 66): the construction of bounded-strength Eulerian (67) and concatenated dynamical-decoupling protocols (68, 69), as well as combinatorial methods for multipartite systems (70, 71); optimized control sequences for the elimination of pure dephasing in a single qubit (72); schemes to reduce specific decoherence mechanisms, such as $1/f$ noise in superconducting devices (73–76), and hyperfine- and phonon-induced decoherence in QDs (77–84); and the compensation of imperfect averaging through the addition of randomized strategies into the dynamical-decoupling design (65, 66, 85–89). Within the field of experimental quantum information processing, dynamical-decoupling techniques have found applications in liquid-state NMR (90) and in solid-state systems such as nuclear quadrupole qubits (91) and fullerene qubits (92) and have inspired charge-based (93) and flux-based (94) echo experiments in superconducting qubits beyond spin systems.

Optical-control, NMR, and dynamical-decoupling methods share the fundamental aspect of controlling quantum dynamics by using pulses that affect phases and therefore the ensuing interference phenomena responsible for quantum dynamics. The methods have emerged from the realm of different scientific communities and continued evolving rather independently for more than 30 years, partially because of the different nature of applications and the different timescales involved. Even the concepts of pulses and phases in the different fields are often used for different physical contexts, making the connection established by common physical principles even less evident. For example, NMR and dynamical-decoupling techniques applied to spin systems

Quantum dot (QD): nanometer semiconducting structure where the charge carriers are confined in all spatial dimensions

Decoherence: suppression of quantum interference due to interactions with the environment

Bang-bang: arbitrarily strong and instantaneous control pulses

Quantum information: field of study that concerns the coding, storage, and transmission of information by exploiting the quantum mechanical properties of light and matter

apply pulses that affect the phase of precession of spins (in a thermal ensemble) relative to an external field, ensuring constructive (or destructive) superposition along a desired direction in space. Therefore, the resulting effect of the pulses is to flip (or orient) the ensemble net polarization in the three-dimensional space. Similarly, pulses of coherent-optical-control schemes change the phases of wave-packet components relative to the other components in a coherent superposition state and therefore rotate ket vector components in Hilbert space to ensure constructive (or destructive) interference in desired (or undesired) quantum states. As a consequence, both coherent-optical-control schemes and dynamical-decoupling methods share common mathematical and physical principles that bridge the gap between the coherent-control and the quantum information communities. It is, therefore, expected that the methods and underlying physical processes reviewed here should be of interest to scientific communities beyond the particular fields in which the techniques were originally developed.

Coherent optical control: active control technique that exploits the coherence property of lasers to manipulate quantum mechanical interferences responsible for dynamical processes

Dynamical decoupling: method to control system dynamics by averaging out internal or external interactions

The review is organized as follows. Section 2 discusses the similarities between coherent-optical-control and dynamical-decoupling methods as contrasted with kinetic control techniques, when applied to controlling quantum dynamics in two-level model systems. Sections 3 and 4 illustrate the application of coherent optical control to the manipulation of decoherence in a model QD and superexchange electron tunneling in functionalized semiconductor nanostructures, respectively. Section 5 discusses dynamical-decoupling schemes for suppressing or accelerating decoherence and for removing unwanted internal interactions.

2. COHERENT OPTICAL CONTROL AND DYNAMICAL DECOUPLING

To illustrate the similarities between coherent-optical-control and dynamical-decoupling methods, we consider two simple models that manipulate the interference between state components in a coherent superposition by using a sequence of unitary pulses. In the first model, a particle in a symmetric double well is described by the following unperturbed Hamiltonian (5, 6):

$$H_0(x, p) = \frac{p^2}{2} - \alpha(x^2 - \beta x^4), \tag{1}$$

where $\alpha = 1/2^2$ and $\beta = 1/2^5$. In the absence of an external perturbation, the initial nonstationary state $\Phi_0(x) = \pi^{-1/4} \exp[-(x - x_0)^2/2]$ (where $x_0 = -4$) evolves in time, tunneling back and forth through the potential energy barrier. In the second model, a spin-1/2 is described by the time-independent Hamiltonian

$$H_0 = B_x \sigma_x, \tag{2}$$

where $\sigma_x, \sigma_y, \sigma_z$ are Pauli matrices and B_x is a magnetic field in the x direction. The initial state $\Phi_0 = |\uparrow\rangle = \binom{1}{0}$, which is an eigenstate of σ_z, evolves in time according to the coherent superposition $\Phi_t = \cos(B_x t)|\uparrow\rangle - i \sin(B_x t)|\downarrow\rangle$, oscillating between the states $|\uparrow\rangle$ and $|\downarrow\rangle$. Coherent dynamical processes in both model systems can be controlled by applying a sequence of instantaneous phase-kick pulses as described in the following sections.

2.1. Coherent Optical Control of Tunneling

The tunneling of a particle in the double-well potential introduced by the first model can be analyzed by considering the evolution of the nonstationary state,

$$|\Phi_0\rangle = \frac{1}{\sqrt{2}}(|\chi_0\rangle + |\chi_1\rangle), \tag{3}$$

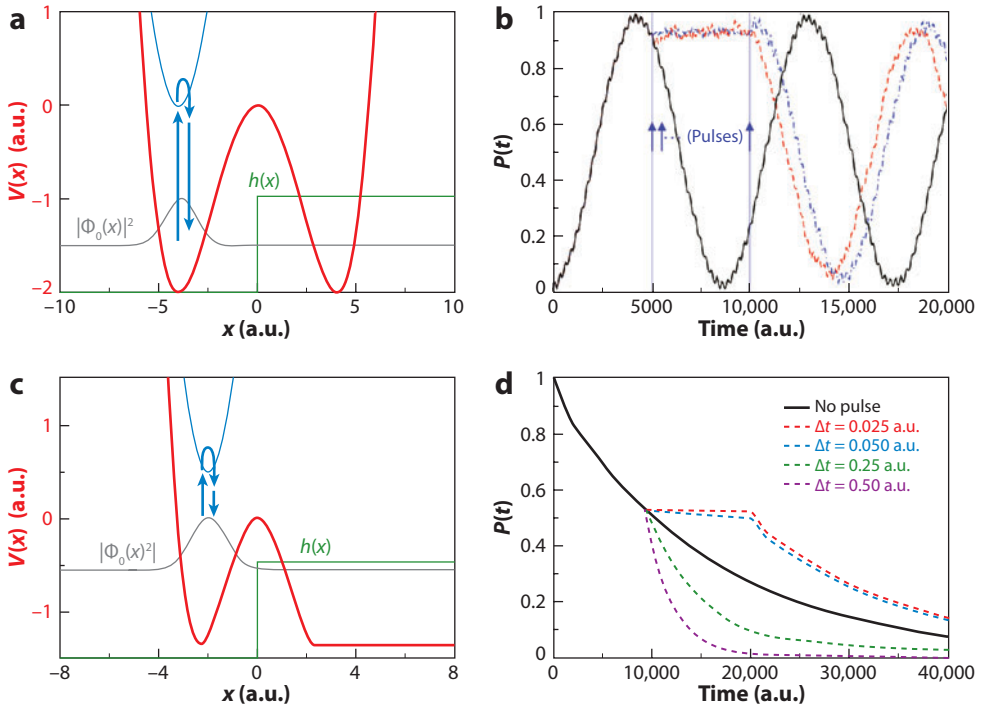

Figure 1

(*a*) Double-well model potential (*red line*), initial state $\Phi_0(x)$ (*gray line*) and tunneling dynamics quantified by (*b*) the time-dependent population $P(t) = \langle \Phi_t | h | \Phi_t \rangle$ on the right side of the tunneling barrier. We compare results in the absence of an external field (*black line*), affected by a sequence of 2π unitary pulses (*blue lines*) stimulating resonance Raman transitions with the auxiliary state (*blue arrows* in panel *a*) during the time window $t = 5000$–$10{,}000$ a.u., and in the presence of a Stark perturbation (*red line*). (*c*) Tunneling barrier model potential (*red line*), initial state $\Phi_0(x)$ (*gray line*), and tunneling dynamics quantified by (*d*) the time-dependent population $P_L(t) = \langle \Phi_t | 1 - h | \Phi_t \rangle$ of the left side of the tunneling barrier. We compare results in the absence of an external field (*black line*) or influenced by a sequence of 2π unitary pulses applied at time intervals $t = 0.025$ (*red*), 0.050 (*blue*), 0.25 (*green*), and 0.50 a.u. (*purple*), stimulating resonance Raman transitions with an auxiliary state (*blue arrows* in panel *c*).

initially localized on the left of the potential energy barrier (see **Figure 1*a***), as defined in terms of the linear combination of the ground and first excited states $|\chi_0\rangle$ and $|\chi_1\rangle$, with $\hat{H}|\chi_j\rangle = E_j|\chi_j\rangle$. In the absence of an external perturbation, $|\Phi_0\rangle$ evolves in time as characterized by the survival amplitude,

$$\xi_t = |\langle \Phi_0 \mid \Phi_t \rangle|^2 = \frac{1}{2} + \frac{1}{2}\cos(\Omega t), \tag{4}$$

tunneling spontaneously back and forth through the potential energy barrier, with a Rabi frequency $\Omega = (E_1 - E_0)/\hbar$. **Figure 1*b*** shows the time-dependent population $P(t) = \langle \Phi_t | h | \Phi_t \rangle$ on the right side of the potential energy barrier, where the Heaviside step function $h(x) = 1$ for $x > 0$ and $h(x) = 0$ otherwise.

Tunneling dynamics can be controlled in the first model by repeatedly applying phase-kick pulses, as shown in **Figure 1*b*** during the time window $t = 5000$–$10{,}000$ a.u. The phase kicks result from ultrafast laser pulses stimulating resonance Raman scattering events (**Figure 1*a***). The pulses couple $|\Phi_0\rangle$ with an auxiliary excited state $|\Phi_a\rangle$, leaving it unpopulated (i.e., $\langle \Phi_a \mid \Phi_t \rangle = 0$)

after and before application of the pulse described by the following operator:

$$\hat{U}^{2\Theta} = \cos\left(\frac{\Gamma\tau}{2}\right)(|\Phi_0\rangle\langle\Phi_0| + |\Phi_a\rangle\langle\Phi_a|) - i\sin\left(\frac{\Gamma\tau}{2}\right)(|\Phi_0\rangle\langle\Phi_a| + |\Phi_a\rangle\langle\Phi_0|), \quad (5)$$

where $\tau = 2\Theta/\Gamma$ is the duration of the pulse of frequency $\Gamma/2$. The results shown in **Figure 1** correspond to 2π pulses, with $\Theta = \pi$. Each pulse introduces a π phase shift along the $|\Phi_0\rangle$ component of the time-evolved wave packet $|\Phi_t\rangle$, and because the auxiliary state remains unpopulated, the 2π pulse can be represented as follows:

$$\hat{U}^{2\pi}(t) = 1 - 2|\Phi_0\rangle\langle\Phi_0|. \quad (6)$$

We consider N sufficiently frequent 2π pulses applied at equally spaced time intervals $\Delta t = 2\tau$, starting at t_0 when $|\Phi_{t_0}\rangle = c_0(t_0)|\Phi_0\rangle + \ldots$, with the remaining terms in the expansion orthogonal to $|\Phi_0\rangle$. The time-evolved state at $t = t_0 + N\Delta t$ can be described by

$$\begin{aligned}|\Phi_{2N\tau+t_0}\rangle &= c_0(t_0)\left(e^{-\frac{i}{\hbar}\hat{H}\tau}\hat{U}^{2\pi}e^{-\frac{i}{\hbar}\hat{H}\tau}\right)^N|\Phi_0\rangle + \ldots \\ &= c_0(t_0)(-1)^N e^{-\frac{i}{\hbar}(E_0+E_1)2N\tau}|\Phi_0\rangle + \ldots, \end{aligned} \quad (7)$$

where the second equality was obtained by substituting $\hat{U}^{2\pi}$ as defined by Equation 6 and $|\Phi_0\rangle$ according to Equation 3. Equation 7 shows that tunneling is completely suppressed during the application of the phase-kick pulses because the population of $|\Phi_0\rangle$ remains constant. However, tunneling is immediately resumed as soon as the sequence of pulses is interrupted.

Similar control methods based on sequences of phase-kick pulses have been applied to control decay and decoherence in other systems (56, 64, 95–97). As an example, **Figure 1*c*,*d*** shows that a sequence of instantaneous 2π pulses can achieve coherent control of spontaneous tunneling decay into a continuum. Here, the effect of a sequence of 2π pulses (applied during the time window $t =$ 10,000–20,000 a.u. at equally spaced time intervals in the $\Delta t = 0.025$–0.5-a.u. range) is quantified by the time-dependent population $P_L(t) = \langle\Phi_t|1 - h|\Phi_t\rangle$ on the left side of the potential energy barrier. **Figure 1*c*** shows that the decay of the metastable initial state can be strongly suppressed by a sequence of sufficiently frequent 2π pulses or otherwise accelerated by less frequent sequences, without changing the potential energy surface responsible for the evolution of quantum dynamics (6). These results are consistent with several other studies of coherent control based on sequences of 2π pulses that were successfully applied to inhibit unwanted transitions (4–6, 96, 98, 99), accelerate decay into a continuum (95), and control the dynamics of molecular orientation (100, 101).

2.2. Dynamical Decoupling of Spin-1/2

Dynamical-decoupling methods (and, more generally, NMR techniques) aim at controlling the dynamics of a system by designing sequences of control pulses based on the desired form of the effective propagator U at time $t > 0$. In general, the design of pulse sequences requires appropriate methods, the most common being the average Hamiltonian theory (66) described in Section 5. For the particular example of the second model above, the goal is to freeze the system evolution by achieving $U(t) \to 1$. It is straightforward to verify that this may be accomplished (apart from a global phase) with a sequence of instantaneous π pulses applied perpendicularly to the x direction, such as $P_z = \exp[-i\pi\sigma_z/2]$, which rotates the spin by 180° around the z direction. The pulses are applied after every time interval Δt of free evolution, so that at $2\Delta t$, we obtain

$$\begin{aligned}U(2\Delta t) &= P_z\exp[-iB_x\sigma_x\Delta t]P_z\exp[-iB_x\sigma_x\Delta t] \\ &= (-1)\exp[-iB_x\exp(i\pi\sigma_z/2)\sigma_x\exp(-i\pi\sigma_z/2)\Delta t]\exp[-iB_x\sigma_x\Delta t] \\ &= (-1)\exp[iB_x\sigma_x\Delta t]\exp[-iB_x\sigma_x\Delta t] = -1. \end{aligned} \quad (8)$$

The effect of pulsing is to reverse the system evolution, canceling out dephasing at times $t = n2\Delta t$, with $n \in N$. Equivalent to the tunneling problem discussed in Section 2.1, the effects of the pulses may also be understood from the perspective of the state of the system. The pulse introduces a phase change to the component $|\downarrow\rangle$ of the coherent superposition, leading to destructive interference and the subsequent restoration of the initial state (apart from a global phase):

$$\begin{aligned}
\psi(0) &= |\uparrow\rangle, \\
U(\Delta t)\psi(0) &= \cos(B_x\Delta t)\,|\uparrow\rangle - i\sin(B_x\Delta t)\rangle, \\
PU(\Delta t)\psi(0) &= (-i)\,[\cos(B_x\Delta t)\,|\uparrow\rangle + i\sin(B_x\Delta t)\,|\downarrow\rangle], \\
U(\Delta t)PU(\Delta t)\psi(0) &= (-i)\,|\uparrow\rangle, \\
PU(\Delta t)PU(\Delta t)\psi(0) &= -|\uparrow\rangle. \qquad (9)
\end{aligned}$$

Section 5 generalizes the dynamical-decoupling scheme briefly introduced here with more complex pulse sequences designed to eliminate noncommuting terms of the Hamiltonian. In the language of optical control, these sequences address scenarios where multiple interfering quantum paths are available.

2.3. Kinetic Control

Control of quantum tunneling dynamics can also be achieved by using kinetic control methods, in which external electromagnetic fields are applied to affect the ensuing quantum dynamics by modulating the potential energy landscape, collapsing the coherent evolution of the system, or inducing mode-selective excitation. To compare coherent-control and kinetic-control methods, we consider the Stark perturbation,

$$H_1(x, t) = \lambda x \sin(\omega t), \qquad (10)$$

that modulates the potential energy landscape of the symmetric double-well potential (the first model system above). The parameters of the perturbation H_1 are chosen with a suitable resonant frequency $\omega = 0.01$ and coupling parameter $\lambda = 0.003171$ (8). **Figure 1*b*** shows that such a time-dependent perturbation, applied during $t = 5000$–$10{,}000$ a.u., inhibits tunneling.

Other kinetic control methods, such as scenarios based on the quantum Zeno effect (10), collapse the coherent quantum evolution of the system owing to the influence of an external perturbation (12, 13). The perturbation can either delay (Zeno effect) or accelerate (anti-Zeno effect) the decoherence process (102). Unifying approaches based on an adiabatic theorem (9), or that consider the quantum measurement theory in detail (11), have been proposed to explain the various forms of Zeno effects.

All the methods discussed in this section belong to the general class of active control scenarios in which the properties of engineered electromagnetic fields are externally manipulated to produce a desired outcome of a dynamical process. The distinctive aspect of coherent-control and dynamical-decoupling methods is that they affect the phases of wave-packet components responsible for interference, without changing the potential energy surface or collapsing the coherent evolution of dynamics. In contrast, kinetic control methods for dynamical localization, or coherent destruction of quantum tunneling, affect the potential energy surface at which the system propagates (7, 8).

Many experimental studies have demonstrated control of quantum dynamics by applying sinusoidal driving potentials. Starting with the use of RF electromagnetic pulse sequences in NMR, RF pulse techniques were subsequently used to achieve coherent control in a wide range of systems, including applications to the renormalization of Landé g factors in atoms (103), the micromotion of single trapped ions (104), the motion of electrons in semiconductor superlattices (105),

the resonance activation of a Brownian particle out of a potential well modeling a current-biased Josephson tunnel junction in its zero-voltage state (1) [also analyzed by theoretical studies (106–111)], and the dynamical suppression of interwell tunneling of a Bose-Einstein condensate in a strongly driven periodic optical potential (112, 113). Several other experiments have also reported tunneling suppression (114, 115), and more recently dynamical localization and coherent suppression of tunneling have been demonstrated for light propagating in coupled waveguide arrays (116, 117). These experimental breakthroughs in the manipulation of oscillatory fields to achieve control suggest that coherent-control scenarios with similar capabilities should be useful in controlling the quantum dynamics of a variety of systems ranging from single atoms and molecules to Bose-Einstein condensates and nanoscale devices (including QDs and QD molecules) and ultimately in controlling quantum superpositions of macroscopically distinct states that can be realized in Josephson junction–based devices. Therefore, the reviewed coherent-control scenarios and dynamical-decoupling methods should raise significant experimental interest, particularly in studies of coherent optical manipulation of electronic excitations in devices in which performance is limited by quantum tunneling and decoherence.

3. COHERENT CONTROL OF DECOHERENCE IN A MODEL QUANTUM DOT

Coherent-control scenarios based on sequences of unitary phase-kick pulses have been recently investigated as applied to controlling decoherence in an electronic QD coupled to a free-standing quasi two-dimensional silicon phonon cavity (see **Figure 2**) (6). The model allows one to investigate coherent control in a system analogous to suspended heterostructures typically built with nanomachining technology (118, 119) that exhibits rich quantum chaotic behavior (120, 121). As an example of such heterostructures, **Figure 2** shows a square 1×1-μm free-standing phonon cavity (50 nm thick), produced by the Cornell Nanofabrication Facility, with a QD of diameter 100–250 nm produced by doping selectively a circular area at the surface of the silicon plate or by suspending metallic gates (122, 123). The results presented in this section correspond to a QD of radius $R = 125$ nm, placed slightly off-center in the phonon cavity at the nonsymmetric position $(x, y) = (0.650, 0.575)$ μm. The position of the QD is important because it determines the nature of the underlying relaxation dynamics owing to the interplay between the symmetries of the circular QD eigenstates and the phonon modes of the rectangular cavity. In particular, the spectrum of energy-level spacing is regular (i.e., described by a Poissonian distribution) when the QD is placed at the center of the cavity $(x, y) = (0.5, 0.5)$ μm (120, 121). However, it exhibits

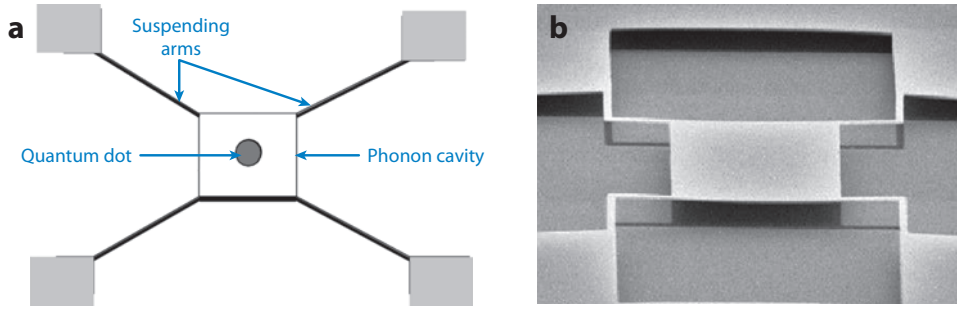

Figure 2

(*a*) Model quantum-dot structure in a free-standing square phonon cavity. (*b*) Free-standing silicon plate, 50 nm thick and 4 μm long, produced by the Cornell Nanofabrication Facility.

a distinct quantum chaotic behavior characterized by a Gaussian Unitary Ensemble of random matrices when the QD is placed at a nonsymmetric position such as $(x, y) = (0.650, 0.575)$ μm (120, 121).

The model Hamiltonian of the QD coupled to the phonon cavity has been described as a sum of electron, phonon, and electron-phonon interactions:

$$\begin{aligned}\hat{H} &= \hat{H}_{el} + \hat{H}_{ph} + \hat{H}_{el\text{-}ph} \\ &= \sum_k E_k b_k^+ b_k + \sum_\alpha \left(\hat{n}_\alpha + \frac{1}{2}\right)\hbar\omega_\alpha + \sum_{k'\alpha k} V_{k'\alpha k} b_{k'}^+ [a_\alpha^+ + a_\alpha] b_{k'},\end{aligned} \tag{11}$$

where the electronic basis states $|k\rangle = |l, \nu\rangle$ correspond to the possible states of an electron in a two-dimensional circular QD, where l is the angular momentum and ν is the radial quantum number. The operators a_α^+ and a_α create and annihilate phonon modes α and define the number operator $\hat{n}_\alpha = a_\alpha^+ a_\alpha$. The electron-phonon coupling terms $V_{k'\alpha k}$ depend on the material properties, as well as the geometry of the structure, carrying information on the symmetry of the nanoelectromechanical system (120, 121). The Hamiltonian of the compound QD-phonon system, therefore, can be written in the basis set of direct products of the one-electron states $|k\rangle$ and the multiphonon states $|n_1 n_2 n_3 \ldots n_N\rangle$, where $n_\alpha = 0, 1, \ldots, n$ denotes the number of phonon quanta in mode α, considering a total of $N = 27$ distinct phonon modes and $n_\alpha \leq 30$. A typical state for the compound system can be represented as

$$|k; \mathbf{n}\rangle = |k\rangle \prod_\alpha^N \frac{1}{\sqrt{n_\alpha!}} \left(a_\alpha^+\right)^{n_\alpha} |0\rangle \,. \tag{12}$$

The dynamics of decoherence has been investigated by computing the time evolution of the electronic angular momentum $L_{el} = Tr\{\hat{\rho}_{el}(t)\hat{L}\}$, where $\hat{\rho}_{el}(t) = Tr_{ph}\{\hat{\rho}(t)\}$ is the reduced electronic density matrix and Tr_{ph} designates the trace over phonon states. The decoherence dynamics was quantified by computing $\Gamma_{el} = Tr\{\hat{\rho}_{el}^2(t)\}$. These calculations required the integration of the time-dependent Schrödinger equation, after diagonalization of the compound QD-phonon Hamiltonian.

The dynamics of decoherence has been manipulated by a coherent-control scenario comprising a sequence of 2π pulses (6). Each pulse is described by the unitary operator,

$$\begin{aligned}\hat{U}^{2\pi} &= (\hat{U}^{2\pi})_{el} \otimes \mathbf{I}_{ph}, \\ &= (\mathbf{I} - 2|\, l = 1, \nu\rangle\langle l = 1, \nu|)_{el} \otimes \mathbf{I}_{ph},\end{aligned} \tag{13}$$

and introduces a π phase shift in the $l = 1$ component of the time-evolved state, with $\boldsymbol{I}_{ph}$ as the identity matrix in the basis set of phonon states.

The initial electronic state was chosen to be the first excited rotational eigenstate, as defined by the undisturbed electronic states of the circular two-dimensional QD of radius R,

$$\phi_k(r, \theta) = \frac{J_{|l|}\left(\alpha_{l\nu}\frac{r}{R}\right)\exp[il\theta]}{\sqrt{\pi}R\left|J_{|l|+1}(\alpha_{l\nu})\right|}, \tag{14}$$

where $k \equiv (l, \nu)$ and $l = 0, \pm 1, \pm 2, \ldots$, with $\alpha_{l\nu}$ as the υ-th root of the Bessel function of order $|l|$, $J_{|l|}(\alpha_{1\upsilon}x)$. The corresponding energies of the one-electron states $|\phi_k\rangle$ are $E_k = \frac{\hbar^2}{2m_e}\frac{\alpha_{l\nu}^2}{R^2}$, where m_e is the electron effective mass. The initial state of the phonon bath was defined according to the density matrix, at finite temperature T,

$$\rho_{nn}^{ph} = \frac{\exp\left(-E_{ph}(\mathbf{n})/k_B T\right)}{\sum_{\{\mathbf{n}\}}\exp\left(-E_{ph}(\mathbf{n})/k_B T\right)}, \tag{15}$$

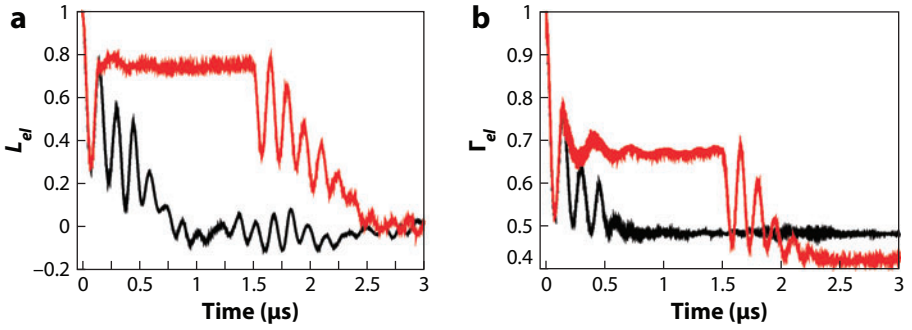

Figure 3

(*a*) Time-dependent angular momentum $L_{el} = Tr\{\hat{\rho}_{el}(t)\hat{L}\}$ and (*b*) decoherence measure $\Gamma_{el} = Tr\{\hat{\rho}^2_{el}(t)\}$ associated with the dynamics of an electron in a quantum-dot structure, coupled to a two-dimensional, free-standing thermal phonon cavity. The freely evolving propagation (*black line*) is compared to the dynamics of the system perturbed by a sequence of 2π pulses, applied at intervals $\Delta\tau = 0.9$ ns during the time window $t = 0.1$–1.5 μs (*red line*).

where $E_{ph}(\mathbf{n}) = \sum_{\alpha}(n_\alpha + \frac{1}{2})\hbar\omega_\alpha$ is the energy of the multimode phonon cavity state $\mathbf{n} \equiv (n_1, n_2, \ldots, n_N)$.

Figure 3 shows the evolution of the time-dependent electronic angular momentum $L_{el} = Tr\{\hat{\rho}_{el}(t)\hat{L}\}$ and the decoherence measure $\Gamma_{el} = Tr\{\hat{\rho}^2_{el}(t)\}$ during the early time relaxation after initializing the electronic state in the first excited rotational state $L_{el} = 1$, with $|k\rangle = |l = 1, \nu = 1\rangle$ in interaction with the phonon bath at $T = 200$ mK. It also shows the evolution of L_{el} and Γ_{el}, corresponding to the dynamics of the system perturbed by a sequence of 2π pulses. The decoherence dynamics is inhibited and ultimately halted by the sequence of phase-kick pulses, without collapsing the evolution of the system. Once the sequence of perturbational pulses is complete (at $t = 1.5$ μs), the decoherence dynamics is reestablished.

The results reviewed in this section show that sequences of phase-kick pulses can be applied to coherently control electronic decoherence in QDs coupled to a thermal bath. When one considers the possibility of engineering this type of semiconductor device that can test quantum tunneling and decoherence phenomena, it is natural to anticipate considerable experimental interest in examining the proposed coherent-control scenario. In particular, QDs have already been recognized as physical realizations of artificial atoms and molecules whose properties (e.g., structural and transport) can be engineered for specific applications and modulated in the presence of external fields (124–126). Proposals include arrays of coupled QDs for applications to create charge or spin qubit gates (48, 49, 127) or quantum memory units (128). However, efficient methods for coherent optical manipulation of decoherence and quantum tunneling dynamics have yet to be established.

4. COHERENT CONTROL OF SUPEREXCHANGE ELECTRON TRANSFER

TiO_2: natural form of titanium oxide, a semiconductor material commonly used in a wide range of applications, including dye-sensitized solar cells

Recent theoretical studies have addressed the feasibility of creating and coherently manipulating electronic excitations in TiO_2 semiconductor surfaces, functionalized with molecular adsorbates (4, 6). These studies aimed at exploring realistic models of molecular qubits based on existing semiconductor materials, building upon previous work focused on the characterization of timescales and mechanisms of interfacial electron transfer in sensitized TiO_2-anatase nanoparticles (129–132) and earlier studies of coherent optical control of molecular processes (29–31, 37).

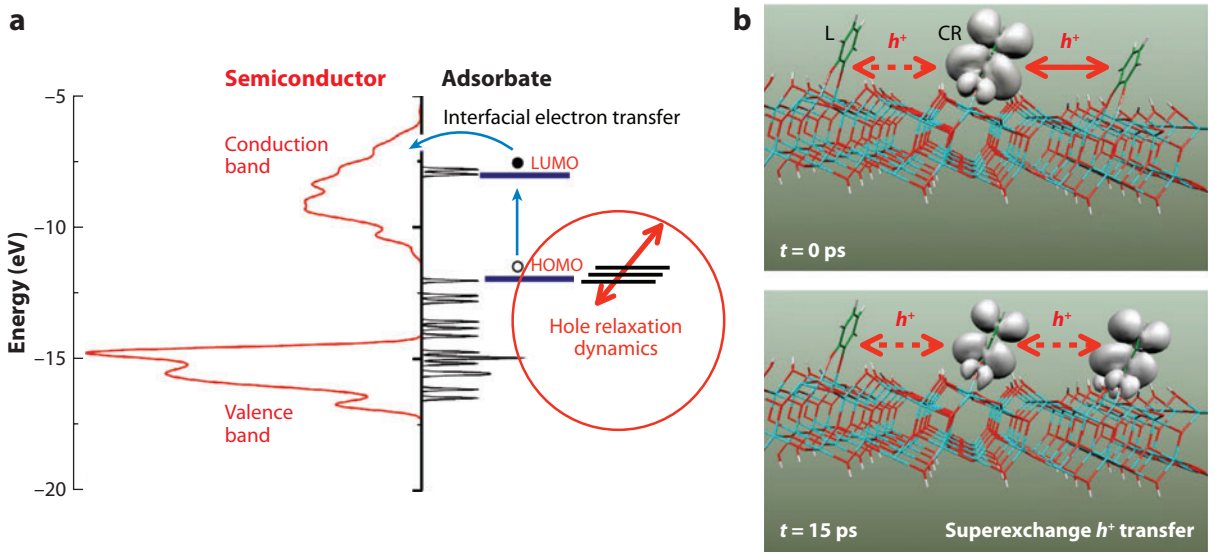

Figure 4

(*a*) Schematic energy diagram of the electronic structure of the TiO_2-anatase surface functionalized with molecular adsorbates, including the valence and conduction bands of TiO_2 and the energy levels due to the molecular adsorbate. The arrows indicate the photoinjection process and the relaxation of the hole in the manifold of near-resonant energy levels localized in the adsorbates. (*b*) TiO_2-anatase functionalized with catechol molecules and isosurface density, representing a nonstationary hole state delocalized on the molecular adsorbates after 15 ps of relaxation dynamics.

Functionalization results from the adsorption of molecules onto the semiconductor surface. As a result, molecules are covalently attached, forming surface complexes that introduce electronic states in the semiconductor band gap (see **Figure 4*a***). The host semiconductor material is thus sensitized to photoabsorption at lower frequencies, characteristic of the molecular adsorbates, leading to ultrafast interfacial electron injection when there is a suitable energy match between the photoexcited electronic states in the surface complex and the electronic states in the conduction band of the semiconductor surface. The resulting photoexcitation and interfacial relaxation process has already raised significant experimental interest because it is central in applications to photovoltaic devices for solar-energy conversion (133, 134) and photocatalysis (129, 135–139).

Recent computational studies have addressed the relaxation dynamics of electron holes left within the semiconductor band gap after photoinduced electron injection (see **Figure 4**) (4, 5, 131). The distinctive aspect of holes localized in these intraband states is that they remain off-resonance relative to the semiconductor (valence and conduction) bands, naturally protected from dissipation into the semiconductor material. However, superexchange hole tunneling into near-resonant states localized in adjacent adsorbate molecules often occurs, even under low-surface-coverage conditions, when the electronic states of the adsorbates are only indirectly coupled by the common host substrate (see **Figure 4**).

Computations of transient hole populations have been based on mixed quantum-classical simulations of dynamics, treating the evolution of electronic states fully quantum mechanically in conjunction with the classical propagation of an ensemble of nuclear trajectories evolving on effective mean-field potential energy surfaces (4, 5, 130, 131).

Figure 5*a* shows the evolution of time-dependent hole populations $P(t)$ of the three adsorbate molecules functionalizing the TiO_2 nanostructure shown in **Figure 4**. $P(t)$ is quantified by the

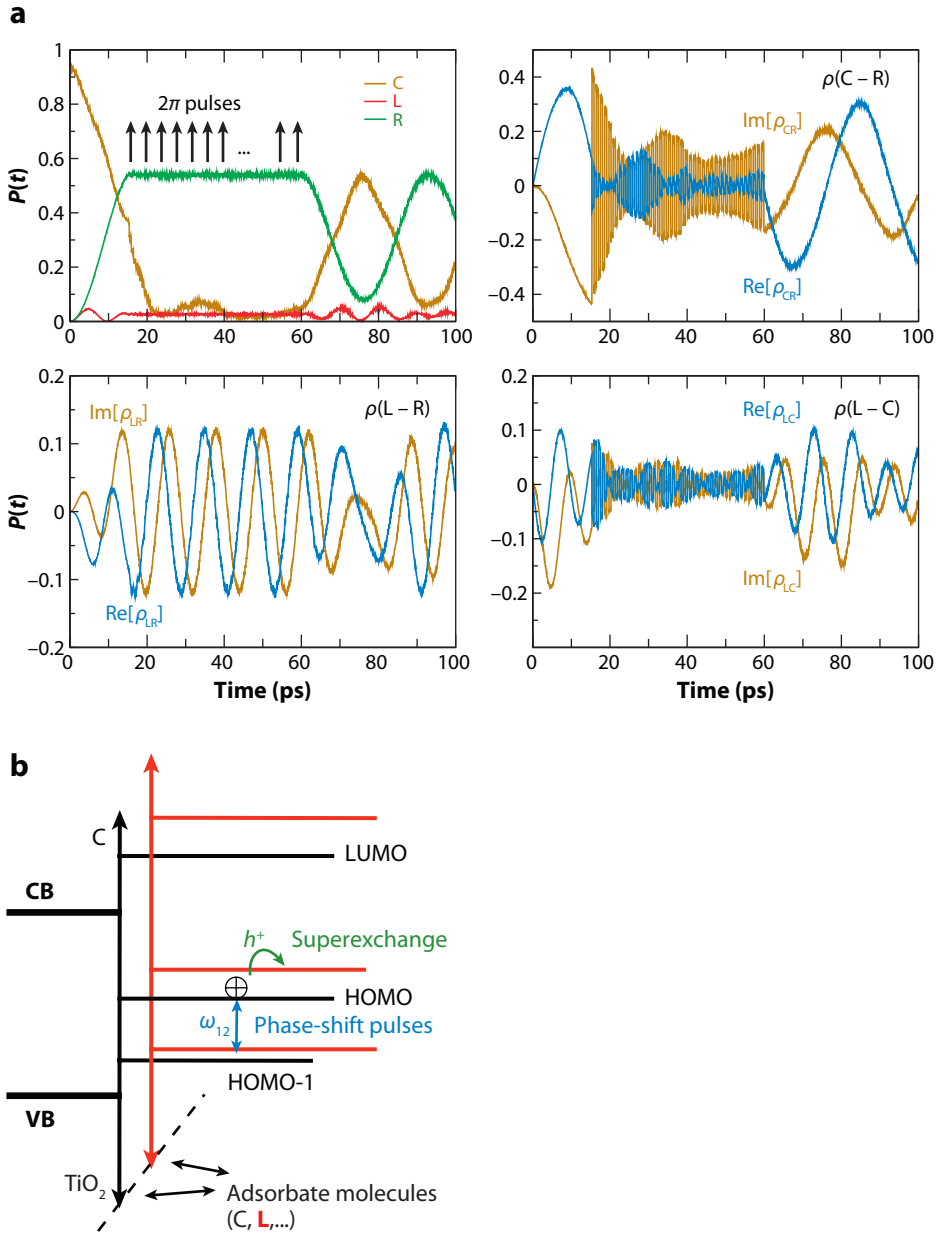

Figure 5

(*a*) Time-dependent hole population *P(t)* for the three adsorbates C, L, and R. The arrows indicate the start and the end of the sequence of 2π pulses. The real (*gold*) and imaginary (*blue*) parts of the off-diagonal elements of the reduced density matrix are indicated by the labels. (*b*) Schematic energy diagram of adsorbate complexes C and L and electronic transitions associated with the coherent control of superexchange hole tunneling based on multiple phase-kick pulses. CB, conduction band; VB, valence band.

diagonal elements of the reduced density matrix $\rho(t)$, associated with the subspace of electronic states localized in the adsorbate molecules $MOL =$ (left, center, right). These results indicate that the hole tunnels between adjacent adsorbate molecules. These are covalently attached to the TiO_2 nanoparticle approximately 1 nm apart from each other. Therefore, the direct electronic coupling is negligible because there is negligible overlap of molecular orbitals. Electronic couplings with off-resonant states in the common host substrate, however, induce superexchange hole tunneling. The underlying relaxation dynamics thus keeps the hole localized in the monolayer of adsorbates rather than injecting it into the semiconductor host substrate. The analysis of individual members of the ensemble indicates that population transfer is most prominent when the electronic states of adjacent adsorbates become near resonant (131). Quantum coherences during the entire simulation time are characterized by the nonzero off-diagonal elements of the reduced density matrix (**Figure 5**) and by the decoherence parameter $Tr[\rho^2(t)]$ (131). These results suggest that the observation of Rabi oscillations, associated with the adsorbate electronic populations, could provide a simple experimental probe of the predicted quantum coherent relaxation dynamics.

Computational studies have addressed the nontrivial question of whether the underlying superexchange hole-tunneling dynamics, associated with electronic relaxation in monolayers of adsorbate molecules, could be coherently controlled by the application of (deterministic and stochastic) sequences of unitary phase-kick pulses (see **Figure 5**) (4, 6). As an example, **Figure 5** shows the perturbational effect of a sequence of 2π pulses on the relaxation dynamics of electron holes undergoing superexchange hole transfer between adsorbate molecules functionalizing a TiO_2 nanoparticle. The pulses are applied during the $t = 15$–60 ps time window at intervals of 550 fs, starting at $t = 15$ ps when there is maximum entanglement between adsorbates C and R [i.e., when the off-diagonal elements $\langle C|\,\rho(t)\,|R\rangle$ are maximum)]. The analysis of off-diagonal elements of the reduced density matrix $\rho(t)$ indicates that the pulse sequence influences the interference between electronic states by rapidly affecting the relative phase of states responsible for relaxation, without collapsing the coherent quantum evolution of the hole. The coherent hole tunneling is reestablished once the sequence of phase-kick pulses is complete. Whereas the results illustrated in **Figure 5** correspond to deterministic sequences of 2π pulses, one can achieve similar coherent control over relaxation dynamics with stochastic 2Θ pulses, where Θ is a random phase. The intervals between pulses can also be varied stochastically so long as the pulses are applied sufficiently frequently (5). These results suggest the feasibility of applying currently available femtosecond laser technology to achieve coherent optical manipulation of electronic excitations in functionalized TiO_2 surfaces, under a wide range of experimental conditions.

5. DYNAMICAL DECOUPLING

This section reviews the basic ideas of dynamical decoupling, including the underlying group theoretical framework, strategies to improve protocol performance, and a brief discussion of relevant frames and the control settings. Throughout, spin-1/2 refers to a model for any two-level system, being therefore frequently exchanged with the more general idea of a qubit. We present two scenarios as illustrative examples: the frozen evolution of an isolated spin-1/2 chain through the removal of unwanted internal interaction (emphasizing the advantages of randomization) and the suppression of decoherence in the case of a single spin-1/2 coupled to a bosonic bath (addressing the phenomena of decoherence acceleration and asymptotic saturation).

5.1. Theoretical Framework

In dynamical-decoupling methods, a time-dependent control Hamiltonian $H_c(t)$ is added to the Hamiltonian $H_0(t)$ of the system whose dynamics we want to modify. The time-evolution operator in the physical (Schrödinger) frame under the total Hamiltonian becomes

$$U(t) = \tau \exp\left[-i \int_0^t [H_0(u) + H_c(u)]du\right], \tag{16}$$

whereas the control propagator is $U_c(t) = \tau \exp[-i \int_0^t H_c(u)du]$, where we set $\hbar = 1$ and τ denotes time ordering. In the ideal case of bang-bang control, the pulses P_k are instantaneous and depend only on $H_c(t)$, whereas during the intervals $\Delta t = t_k - t_{k-1}$ between control operations, the system evolves freely according to $H_0(t)$. The propagator at $t_n = n\Delta t$, $n \in N$, is then

$$\begin{aligned} U(t_n) &= P_n U(t_n, t_{n-1}) P_{n-1} U(t_{n-1}, t_{n-2}) \ldots P_1 U(t_1, 0) P_0 \\ &= \underbrace{(P_n P_{n-1} \ldots P_1 P_0)}_{U_c(t_n)} \underbrace{(P_{n-1} \ldots P_1 P_0)^+ U(t_n, t_{n-1})(P_{n-1} \ldots P_1 P_0) \ldots (P_1 P_0)^+ U(t_2, t_1)(P_1 P_0) P_0^+ U(t_1, 0) P_0}_{\tilde{U}(t_n)}, \end{aligned} \tag{17}$$

where $\tilde{U}(t_n)$ stands for the evolution operator in the logical frame

$$\tilde{U}(t) = \tau \exp\left[-i \int_0^t \tilde{H}(u)du\right], \quad \text{and} \quad \tilde{H}_0(t) = U_c^+(t) H_0(t) U_c(t). \tag{18}$$

The logical (also known as toggling) frame corresponds to a time-dependent interaction representation that follows the control. It is a theoretical tool often used in the design of dynamical-decoupling protocols along with the average Hamiltonian theory (18, 19). The latter consists of writing the logical propagator in terms of a single exponential and identifying the appropriate sequence of pulses leading to the desired form of the effective propagator at a final time t_n. For a time-independent system Hamiltonian H_0, we find

$$\tilde{U}(t_n) = \exp[-i\tilde{H}_n \Delta t] \ldots \exp[-i\tilde{H}_2 \Delta t] \exp[-i\tilde{H}_1 \Delta t] = \exp\left[-i \sum_{k=0}^{\infty} \left(\bar{H}^{(k)}(t_n)\right) t_n\right], \tag{19}$$

where $\tilde{H}_n = (P_{n-1} \ldots P_1 P_0)^+ H_0 (P_{n-1} \ldots P_1 P_0)$ are transformed Hamiltonians, and the Baker-Campbell-Hausdorff expansion was used to derive the last equality [the Magnus expansion (18, 19) is required when dealing with a time-dependent system Hamiltonian]. Each $\bar{H}^{(k)}(t_n)$ is proportional to $(\Delta t)^k / t_n$ and involves k time-ordered commutators of transformed Hamiltonians.

For cyclic control with cycle time T_c [that is, $H_c(t + nT_c) = H_c(t)$ and $U_c(t + nT_c) = U_c(t)$], the physical and logical frames coincide at every $T_n = nT_c$; therefore, $U(nT_c) = \tilde{U}(nT_c)$. At these instants, the system appears to evolve under a time-independent average Hamiltonian $\bar{H} = \sum_{k=0}^{\infty} \bar{H}^{(k)}$ leading to $\tilde{U}(nT_c) = \tilde{U}(T_c)^n = \exp[-i\bar{H}nT_c]$. Thus, to analyze the system evolution at T_n it suffices to derive the propagator at T_c. Pulse sequences are then constructed based primarily on the appropriate form of the dominant terms in the average Hamiltonian. Given $T_c = M\Delta t$, where M is a number determined by the sequence considered, the three first dominant terms are

$$\bar{H}^{(0)} = \frac{\Delta t}{T_c} \sum_{k=1}^{M} \tilde{H}_k, \tag{20}$$

$$\bar{H}^{(1)} = -i \frac{(\Delta t)^2}{2T_c} \sum_{l=2}^{M} \sum_{k=1}^{l-1} [\tilde{H}_l, \tilde{H}_k], \tag{21}$$

$$\tilde{H}^{(2)} = -\frac{(\Delta t)^3}{6T_c}\left\{\sum_{m=3}^{M}\sum_{l=2}^{m-1}\sum_{k=1}^{l-1}\{[\tilde{H}_m,[\tilde{H}_l,\tilde{H}_k]]+[[\tilde{H}_m,\tilde{H}_l],\tilde{H}_k]\}\right.$$
$$\left.+\frac{1}{2}\sum_{l=2}^{M}\sum_{k=1}^{l-1}\{[\tilde{H}_l,[\tilde{H}_l,\tilde{H}_k]]+[[\tilde{H}_l,\tilde{H}_k],\tilde{H}_k]\}\right\}. \quad (22)$$

For short times and in the limit $T_c \to 0$, reshaping the Hamiltonian based on the dominant terms leads to dynamics close enough to the desired one.

In NMR spectroscopy, the design of control protocols usually aims at specific systems. Another approach, often considered in the field of quantum information, invokes group theory (55, 57), in which the purpose is to map the dominant term $\bar{H}^{(0)}$ into a group-theoretic average $\bar{H}_G$. The pulses are successively drawn from a discrete dynamical-decoupling group $G = \{g_j\}$, $j = 0, 1, \ldots, |G| - 1$, where $|G|$ is the size of the group and $T_c = |G|\Delta t$, so that

$$\tilde{U}(T_c) = \prod_{j=0}^{|G|-1} U_{j+1}, \quad (23)$$

with

$$U_{j+1} = g_j^+ U(t_{j+1}, t_j) g_j, \quad \tilde{H}_{j+1} = g_j^+ H_0 g_j, \quad P_{j+1} = g_{j+1} g_j^+, \quad P_0 = g_0,$$

and

$$\bar{H}_G = \frac{1}{|G|}\sum_{k=1}^{|G|}\tilde{H}_k = \bar{H}^{(0)}. \quad (24)$$

In order to freeze the system evolution and achieve $\tilde{U}(T_c) \to 1$, the primary goal becomes first-order decoupling, that is, guaranteeing that at least $\bar{H}^{(0)} = 0$. To illustrate the method, we consider the simplest possible system, that of a single spin-1/2 (qubit) in two situations: (*a*) $H_0 = B_z\sigma_z$ and (*b*) $H_0 = \vec{B}\cdot\vec{\sigma} = B_x\sigma_x + B_y\sigma_y + B_z\sigma_z$, where $\sigma_x, \sigma_y, \sigma_z$ are Pauli matrices; B_z is a magnetic field in the z direction; and $\vec{B}$ is a magnetic field in a supposedly unknown direction.

To freeze the first situation, one needs to frequently undo the phase evolution by rotating the spin 180° around a direction perpendicular to z. This may be accomplished with a sequence of π pulses $P_x = \exp[-i\pi\sigma_x/2]$ applied after every Δt, as determined by the group $G = \{1, \sigma_x\}$. Cyclicity is ensured by subjecting the system to an even number of pulses. Because the two transformed Hamiltonians ($\tilde{H}_1 = B_z\sigma_z$ and $\tilde{H}_2 = B_z\sigma_x\sigma_z\sigma_x = -B_z\sigma_z$) commute, exact cancellation of all orders (k) in the average Hamiltonian is achieved at every T_c, leading to $\tilde{U}(nT_c) = U(nT_c) = 1$. This ideal result does not hold when dealing with realistic finite pulses, in which case $\bar{H} \neq 0$, and special strategies have been developed to eliminate the dominant terms in $\bar{H}$ (19, 67).

In general, however, even when the system is subjected to bang-bang pulses, the transformed Hamiltonians do not commute. This is the case of the second situation listed above. Here, the cancellation of $\bar{H}^{(0)}$ requires alternating 180° rotations of the spin around two perpendicular axes, so that each cycle consists of four pulses. An option corresponds to having $P_1 = P_3 = \exp[-i\pi\sigma_x/2]$ and $P_2 = P_4 = \exp[-i\pi\sigma_y/2]$, although any other path chosen to traverse the group $G = \{1, \sigma_x, \sigma_z, \sigma_y\}$ is also viable. The four noncommuting transformed Hamiltonians ($\tilde{H}_1 = B_x\sigma_x + B_y\sigma_y + B_z\sigma_z$, $\tilde{H}_2 = B_x\sigma_x - B_y\sigma_y - B_z\sigma_z$, $\tilde{H}_3 = -B_x\sigma_x - B_y\sigma_y + B_z\sigma_z$, and $\tilde{H}_4 = -B_x\sigma_x + B_y\sigma_y - B_z\sigma_z$) lead to $\bar{H}^{(0)} = 0$, but $\bar{H}^{(1)} \neq 0$. A deterministic pulse sequence, which guarantees only first-order decoupling, has been named periodic dynamical decoupling (PDD).

5.2. Strategies to Improve Protocol Performance

The design of dynamical decoupling protocols aims at increasing averaging accuracy in the effective Hamiltonian and at slowing down the accumulation of residual averaging errors. Here, we give an overview of some deterministic and randomized strategies to achieve these goals and discuss the advantages of combining both approaches.

5.2.1. Deterministic schemes. Strategies exist to push beyond PDD and eliminate or reduce higher-order terms in $\bar{H}$. Time symmetrization, for instance, corresponds to reversing the pulse sequence, so that at every $T_n = 2nT_c$, $\bar{H}^{(1)}$ and all odd terms in $\bar{H}$ are cancelled. In the second example above, any of the possible PDD sequences $[\tilde{U}(T_c) = U_s \cdot U_r \cdot U_q \cdot U_p$, with $p \in \{1, 2, 3, 4\}$, $q \in \{1, 2, 3, 4\} - \{p\}$, $r \in \{1, 2, 3, 4\} - \{p, q\}$, and $s \in \{1, 2, 3, 4\} - \{p, q, r\}]$ leads to

$$\bar{H}^{(1)} = \frac{-i(\Delta t)^2}{2T_c} \left\{ [\tilde{H}_s, \tilde{H}_r] + [\tilde{H}_q, \tilde{H}_p] \right\}, \tag{25}$$

where the above simplified form was obtained by using the equality

$$\tilde{H}_p + \tilde{H}_q + \tilde{H}_r + \tilde{H}_s = 0. \tag{26}$$

It is straightforward to verify that the symmetric sequence $\tilde{U}(2T_c) = U_p \cdot U_q \cdot U_r \cdot U_s \cdot U_s \cdot U_r \cdot U_q \cdot U_p$ leads to $\bar{H}^{(1)} = 0$.

Whenever the basic PDD sequence requires only four pulses, second-order decoupling may also be achieved by swapping the elements in pairs of subsequent transformed Hamiltonians during the interval $[4\Delta t + 8n\Delta t, 8\Delta t + 8n\Delta t]$ so that

$$\tilde{U}(2T_c) = U_r \cdot U_s \cdot U_p \cdot U_q \cdot U_s \cdot U_r \cdot U_q \cdot U_p. \tag{27}$$

One may further extend this last alternative to achieve third-order decoupling at every $T_n = 6nT_c$. Using Equation 26, $\bar{H}^{(2)}$may be written

$$\bar{H}^{(2)} = \frac{-(\Delta t)^3}{6T_c} \left\{ \left[(2\tilde{H}_p + \tilde{H}_q), [\tilde{H}_p, \tilde{H}_q] \right] + \left[(2\tilde{H}_s + \tilde{H}_r), [\tilde{H}_s, \tilde{H}_r] \right] \right\}. \tag{28}$$

This term is suppressed with a supercycle scheme built up by arranging three $8\Delta t$ sequences:

$$\tilde{U}(6T_c) = (U_q \cdot U_s \cdot U_r \cdot U_p \cdot U_s \cdot U_q \cdot U_p \cdot U_r) \cdot (U_p \cdot U_s \cdot U_q \cdot U_r \cdot U_s \cdot U_p \cdot U_r \cdot U_q) \cdot (U_r \cdot U_s \cdot U_p \cdot U_q \cdot U_s \cdot U_r \cdot U_q \cdot U_p).$$

We refer to this protocol as the H2 scheme.

Concatenation (68, 69) and cyclic permutations (66) are other examples of strategies to improve protocol performance. In four-pulse sequences, half the concatenation procedure at the second level coincides with Equation 27 (66), whereas cyclic permutations are inspired by the MLEV decoupling sequence in NMR (140, 141). In the particular case of a single spin-1/2 system, concatenation has proven to be the most efficient scheme (82–84), a fact associated with the irreducibility of the group considered (66). This should be contrasted with the reducible group employed in Section 5.4, in which we find (in increasing order of performance) time symmetrization, concatenation, cyclic permutations, and the H2 scheme (66).

In periodically repeated sequences, the accumulation of residual errors caused by imperfect averaging is coherent (quadratic in time) and therefore extremely detrimental for long time evolutions. The key ingredient for efficient averaging at long times is the frequent scrambling of the order of the applied dynamical-decoupling pulses, an idea already implicit in concatenation and cyclic permutation and entirely at the heart of randomized methods.

5.2.2. Randomized schemes. The most straightforward randomized dynamical-decoupling protocol is obtained by picking elements uniformly at random over the decoupling group G, such that the control action at each $t_n = n\Delta t$ ($t_0 = 0$ included) corresponds to $P^{(r)} = g_i g_j^+$, where $i, j = 0, 1, \ldots, |G| - 1$. Such scheme is expected to outperform deterministic protocols at long times but not at short times. One can construct high-level randomized protocols, ensuring good performance at both short and long times, by merging together advantageous deterministic and stochastic features. One option consists of selecting a deterministic sequence that guarantees high power of Δt in the effective average Hamiltonian and embedding it with random pulses (85), which slows down error accumulation. Another alternative consists of randomly choosing at every $T_n = n|G|\Delta t$ a control path to traverse the group (88); this sequence may be further improved if it is time symmetrized (66, 87).

A main characteristic of randomized methods is the great variety of control realizations; analyses of protocol performance are then based on averages over large samples of realizations. This enormous number of possible control realizations associated with large systems and long final times hinders the search for optimal deterministic sequences at arbitrary times and favors randomization.

5.3. Frames and Control

The theoretical design of pulse sequences and the evaluation of their performances are usually completed in the logical frame, whereas experiments are actually performed in the physical frame. These differences are disregarded when dealing with periodic sequences because the two frames coincide at the end of each cycle, but acyclic sequences (as randomized schemes) may require a frame-correcting pulse before data acquisition (66, 87, 89).

In realistic control settings, to modify the system dynamics, one couples the system, for instance, to an oscillating control field linearly polarized in the x direction according to

$$H_c(t) = 2\Omega(t)\cos[\omega_f t + \varphi(t)]\frac{X}{2}, \tag{29}$$

where X, Y, and Z correspond to σ_x, σ_y, and σ_z, respectively, in the case of a single spin-1/2 system and to $\sum_{i=1}^{N}\sigma_{x,i}$, $\sum_{i=1}^{N}\sigma_{y,i}$, and $\sum_{i=1}^{N}\sigma_{z,i}$, respectively, for a system of N spins-1/2. The experimentalist has control of the amplitude (power) 2Ω, the carrier frequency ω_f, and the phase φ, as well as the interval τ during which $H_c(t)$ is on, and the separation Δt between successive pulses.

All the results of this section are provided in a frame rotating with the frequency ω_f of the carrier. In this frame, by using the rotating wave approximation, the control Hamiltonian becomes

$$H_c^R(t) = \Omega(t)\left[\frac{X}{2}\cos\varphi(t) + \frac{Y}{2}\sin\varphi(t)\right]. \tag{30}$$

The control field is applied in resonance with the frequency of the spin we want to rotate. The phase φ determines the direction around which the rotation is realized in the rotating frame, and, in the case of rectangular pulses, $\Omega\tau$ characterizes the rotation angle. For example, a π pulse around the x direction requires $\Omega\tau = \pi$ and $\varphi(t) = 0$.

In the idealized scenario of bang-bang pulses (as considered here), the power is infinity and the pulse duration is zero. However, a complete analysis of dynamical-decoupling protocols also requires the consideration of nonidealities such as finite pulses, flip-angle errors, and transients (19, 66), as well as pulse shapes (142–144).

5.4. Isolated Heisenberg Spin-1/2 System with Nearest-Neighbor Interactions

Here we show the advantages of randomization in dynamical-decoupling methods applied for the case of a chain with N spin-1/2 particles (qubits) coupled via isotropic nearest-neighbor interactions, as described by the Heisenberg model:

$$H_0 = H_Z + H_{NN} = \sum_{i=1}^{N} \frac{\omega_i}{2}\sigma_{z,i} + \sum_{i=1}^{N-1} J\vec{\sigma}_i.\vec{\sigma}_{i+1}, \tag{31}$$

where ω_i is the Zeeman splitting energy of qubit i, J is the coupling parameter between the spins, and open boundary conditions are assumed. This Hamiltonian models quasi-one-dimensional magnetic compounds (145) and Josephson junction arrays (146). It is also a fairly good approximation for couplings that decay with the distance between the qubits (for cubic decay, see 87).

Our goal is to freeze the evolution of the system for long times. We assume the possibility of individually addressing the spins with selective pulses and study the system in a combined logical-rotating frame, whereby one-body terms are removed from the Hamiltonian, so that $\tilde{H}_0^R \approx H_{NN}$. First-order decoupling can be achieved through a simple system-size-independent scheme whose cycle is closed after four collective pulses. The sequence has one direction associated with odd qubits and the other direction linked to even ones. A possible representation of the control group for N even is then given by

$$G = \{1, \sigma_{z,1}\sigma_{z,3}\ldots\sigma_{z,N-1}, \sigma_{z,1}\sigma_{y,2}\sigma_{z,3}\sigma_{y,4}\ldots\sigma_{z,N-1}\sigma_{y,N}, \sigma_{y,2}\sigma_{y,4}\ldots\sigma_{y,N}\}. \tag{32}$$

The path leading to the pulses $P_1 = P_3 = \exp(-i\pi\sum_{j=1,3}^{N-1}\sigma_{j,z}/2)$ and $P_2 = P_4 = \exp(-i\pi\sum_{j=2,4}^{N}\sigma_{j,y}/2)$ gives the four transformed Hamiltonians:

$$\begin{aligned}
\tilde{H}_1 &= \sum_{i=1}^{N-1} J\sigma_{x,i}\sigma_{x,i+1} + \sum_{i=1}^{N-1} J\sigma_{y,i}\sigma_{y,i+1} + \sum_{i=1}^{N-1} J\sigma_{z,i}\sigma_{z,i+1},\\
\tilde{H}_2 &= -\sum_{i=1}^{N-1} J\sigma_{x,i}\sigma_{x,i+1} - \sum_{i=1}^{N-1} J\sigma_{y,i}\sigma_{y,i+1} + \sum_{i=1}^{N-1} J\sigma_{z,i}\sigma_{z,i+1},\\
\tilde{H}_3 &= \sum_{i=1}^{N-1} J\sigma_{x,i}\sigma_{x,i+1} - \sum_{i=1}^{N-1} J\sigma_{y,i}\sigma_{y,i+1} - \sum_{i=1}^{N-1} J\sigma_{z,i}\sigma_{z,i+1},\\
\tilde{H}_4 &= -\sum_{i=1}^{N-1} J\sigma_{x,i}\sigma_{x,i+1} + \sum_{i=1}^{N-1} J\sigma_{y,i}\sigma_{y,i+1} - \sum_{i=1}^{N-1} J\sigma_{z,i}\sigma_{z,i+1}.
\end{aligned} \tag{33}$$

Among the deterministic strategies described in Section 5.2.1, the supercycle H2 sequence

$$\tilde{U}(6T_c) = U_2\cdot U_4\cdot U_3\cdot U_1\cdot U_4\cdot U_2\cdot U_1\cdot U_3\cdot U_1\cdot U_4\cdot U_2\cdot U_3\cdot U_4\cdot U_1\cdot U_3\cdot U_2\cdot U_3\cdot U_4\cdot U_1\cdot U_2\cdot U_4\cdot U_3\cdot U_2\cdot U_1 \tag{34}$$

is by far the best deterministic protocol because it is the only one guaranteeing third-order decoupling; that is, it eliminates $\tilde{H}^{(0)}$, $\tilde{H}^{(1)}$, and also $\tilde{H}^{(2)}$. **Figure 6** compares the performance of this efficient deterministic protocol with two randomized schemes: an H2 sequence embedded with random pulses characterized by products of π rotations performed at arbitrarily selected spins around any of the three randomly chosen directions (x, y, or z) and a third-order decoupling sequence in which the path for the interval $[24n\Delta t, 24n\Delta t + 4\Delta t]$ is picked at random.

The quantity considered to quantify protocol performance is the input-output fidelity

$$F(t) = |\langle\psi(0)|U(t)|\psi(0)\rangle|^2, \tag{35}$$

where we consider as the initial pure state an eigenstate of a random matrix belonging to a Gaussian Orthogonal Ensemble.

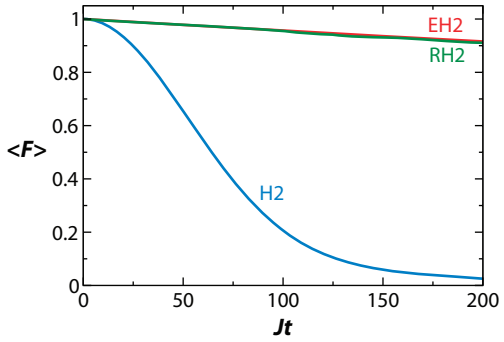

Figure 6

System described by $\tilde{H}_0^R \approx H_{NN}$ with $N = 8$. Data acquired at $T_n = 24n\Delta t$, $\Delta t = 0.1J^{-1}$. The blue line represents a deterministic H2 scheme leading to $\bar{H}^{(0)}, \bar{H}^{(1)}, \bar{H}^{(2)} = 0$; the green line represents the randomized protocol RH2 constructed by randomly choosing a group path for each interval $[24n\Delta t, 24n\Delta t + 4\Delta t]$; and the red line represents the randomized protocol EH2 obtained by embedding the H2 sequence with random pulses. The angled brackets denote an average over 100 realizations.

At long times, the randomized protocols are significantly better, with the fidelity decay much slower than for the deterministic method. Both schemes, embedding the deterministic sequence with random pulses or applying path randomization, showed similar performance, but whether it is better to consider one or the other depends on the system at hand (66, 87, 88). Even though an optimal deterministic sequence may exist for a particular system at a specific final time, identifying it may be hard, in which case resorting to a simple yet efficient randomized sequence, such as the ones described here, is a more practical strategy.

5.5. Suppression of Decoherence: Spin-1/2 Coupled to a Bosonic Bath

Let us consider a target system S consisting of a spin-1/2 (qubit) coupled to a bosonic environment E corresponding to independent harmonic modes, as described by the total Hamiltonian

$$H_0 = H_S + H_E + H_{SE}, \tag{36}$$

where

$$\begin{aligned} H_S &= \frac{\omega_0}{2}\sigma_z, \\ H_E &= \sum_k \omega_k b_k^+ b_k, \\ H_{SE} &= \sigma_z \sum_k g_k (b_k^+ + b_k), \end{aligned} \tag{37}$$

ω_0 is the Zeeman splitting of the spin, b_k^+ and b_k denote creation and annihilation bosonic operators of the environmental mode k with frequency ω_k, and g_k determines the coupling parameter between the system and mode k. The system-bath coupling H_{SE} leads to a purely dephasing process, with the spin population unaffected by the environment. The advantage of such a simple model is that it allows for exact analytical derivations.

The purpose of dynamical decoupling here is to average out the evolution generated by H_{SE} and prevent decoherence. After every Δt, the deterministic sequence corresponds to subjecting the system to a pulse $P_x = \exp[-i\pi\sigma_x/2]$, whereas for the randomized scheme, we choose at random whether the spin is rotated. Studies of protocol performance are based on the behavior of the off-diagonal elements of the reduced density matrix ρ_{01}, which is obtained after tracing over

the degrees of freedom of the reservoir; ρ_{01} contains all relevant phase information. The analysis is developed in a frame that removes both the control field and the free evolution due to H_S, which is referred to as logical–interaction picture frame.

By assuming that the system and the environment are initially uncorrelated and that the bath is in thermal equilibrium at temperature T (the Boltzmann constant is set equal to 1), the expression for the system coherence in the logical–interaction picture frame at time $t_n = n\Delta t$ is given by

$$\tilde{\rho}_{01}^{I}(t_n) = \rho_{01}(0)\exp[-\Gamma(t_n)], \tag{38}$$

where $\Gamma(t_n)$ is the decoherence function. For an ohmic bath in the continuum limit, we find, in the absence of control,

$$\Gamma(t_n) = \alpha \int_0^\infty d\omega \omega e^{-\omega/\omega_c} \coth\left(\frac{\omega}{2T}\right) \frac{1-\cos[\omega t_n]}{\omega^2}; \tag{39}$$

for the deterministic scheme (56, 76),

$$\Gamma(t_n) = \alpha \int_0^\infty d\omega \omega e^{-\omega/\omega_c} \coth\left(\frac{\omega}{2T}\right) \frac{1-\cos[\omega t_n]}{\omega^2} \tan^2\left(\frac{\omega \Delta t}{2}\right); \tag{40}$$

and for the randomized scheme (65),

$$\Gamma(t_n) = \alpha \int_0^\infty d\omega \omega e^{-\omega/\omega_c} \coth\left(\frac{\omega}{2T}\right) \frac{1-\cos[\omega t_n]}{\omega^2} \left[n + 2\sum_{k=1}^{n-1} \cos(k\omega\Delta t) \sum_{l=0}^{n-k-1} \chi_l \chi_{l+k}\right], \tag{41}$$

where α is the interaction strength between the system and the bath, ω_c is an ultraviolet cutoff frequency, and χ_k is a Bernoulli random variable that accounts for the history of spin flips up to t_k in a given realization (it takes the values $+1$ or -1 with equal probability) (65).

Figure 7 compares the three decoherence functions above, considering both high- and low-temperature baths. **Figure 7*a*** shows the high-temperature limit, which corresponds to an

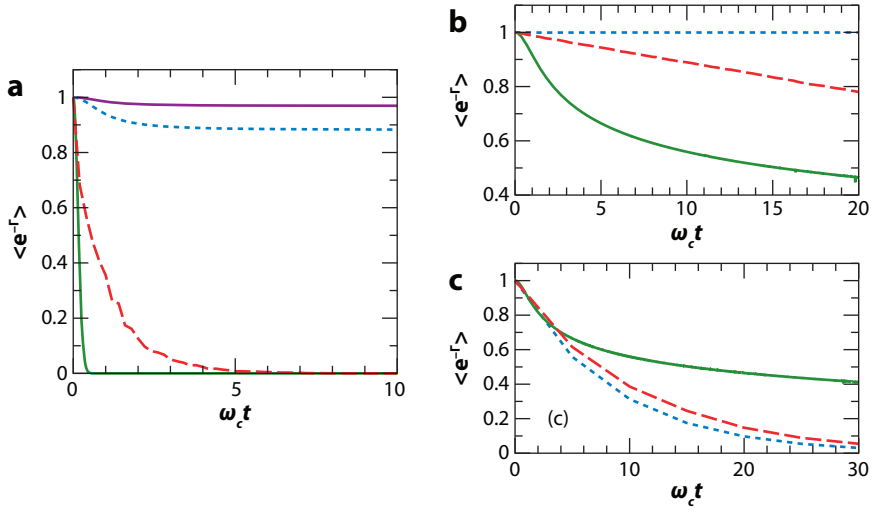

Figure 7

Decoherence rate from a bosonic ohmic bath in units of T^{-1} ($\alpha = 0.25$ and $\omega_c = 100$): (*a*) $T = 100\omega_c$ and $\omega_c \Delta t = 0.1$, (*b*) $T = 0.01\omega_c$ and $\omega_c \Delta t = 0.1$, and (*c*) $T = 0.01\omega_c$ and $\omega_c \Delta t = 2.5$. The green solid line represents no control, the red dashed line is a randomized scheme, the blue dotted line is a deterministic sequence, and the purple solid line is a deterministic sequence with $\omega_c \Delta t = 0.05$. The angled brackets denote an average over 100 realizations.

effectively classical bath dominated by thermal fluctuations. In the absence of control, decoherence is very fast on the timescale determined by the bath correlation time $\tau_c = \omega_c^{-1}$, and coherence preservation requires very short intervals between pulses. When the bath is at low temperature (**Figure 7*b*,*c***), decoherence is slower, and a rich interplay between thermal and vacuum fluctuations occurs. Larger values of Δt may be analyzed before total coherence loss takes place.

5.5.1. Decoherence freezing. For short intervals between pulses ($\omega_c \Delta t \ll 1$) and at long times ($\omega_c t_n \gg 1$), $\Gamma(t_n)$ obtained with the deterministic sequence becomes independent of t_n. It is given by $\Gamma(t_n) = O(\alpha T \omega_c \Delta t^2)$ in the case of high temperatures and by $\Gamma(t_n) = O(\alpha \omega_c^2 \Delta t^2)$ in the case of low temperatures (Equation 40). This asymptotic saturation is verified in **Figure 7*a*,*b***, where $\omega_c \Delta t = 0.1$. The deterministic protocol eventually freezes decoherence at long times. This saturation was also verified in studies of an electron spin decohered by a nuclear spin environment in a QD (82–84). In NMR, saturation is associated with the pedestals seen in the long-time magnetization signal under pulsed spin-locking conditions (19).

5.5.2. Low-temperature bath and decoherence acceleration. The phenomenon of decoherence acceleration, in which pulses induce destructive interference (56, 64), happens when the interval between pulses is larger than the correlation time of the bath, $\omega_c \Delta t > 1$ (**Figure 7*c***). In experimental situations in which the cutoff frequency of the reservoir cannot be overcome by the pulsing frequency, it is therefore better not to perturb the system. We discuss a similar scenario in Section 2.1, showing that tunneling becomes accelerated when the applied sequences of 2π pulses are not sufficiently frequent.

5.5.3. Randomization and stability. In **Figure 7**, whenever $\omega_c \Delta t < 1$, the randomized protocol is outperformed by the deterministic scheme. For the simple model of a single spin interacting with its environment, efficient deterministic protocols have been identified for bosonic (72) as well as fermionic reservoirs (68, 69, 82–84). Yet the advantages of randomization in these models become perceptible when the system Hamiltonian is time dependent and little knowledge about it is available; randomization may then allow for enhanced stability against parameter variations (65). For the case of a time-dependent system with more than one qubit, Reference 87 illustrates the robustness of randomized schemes.

SUMMARY POINTS

1. The development of practical methods for controlling quantum dynamics with electromagnetic fields has a long history and remains an outstanding challenge of great technological interest.
2. Coherent-optical-control, NMR, and dynamical-decoupling methods have emerged from the realm of different scientific communities and evolved rather independently for more than 30 years, partially because of the different nature of applications and different timescales involved. However, considering the common physical principles reviewed in this article, it is natural to expect that these control methods should be of interest to scientific communities beyond the particular fields in which they were originally developed.
3. Coherent-optical-control, NMR, and dynamical-decoupling methods share the common goal of controlling quantum dynamics through the use of unitary pulses. These pulsing schemes can affect the phases and therefore the ensuing interference phenomena in a wide

range of systems, without necessarily changing the potential energy surfaces responsible for quantum dynamics, or collapsing the coherent unitary evolution of the system.

4. The reviewed simulations of coherent optical control suggest the feasibility of applying currently available femtosecond laser technology to effectively suppress or accelerate the quantum tunneling, or decoherence, of electronic excitations in QDs and functionalized TiO_2 surfaces.
5. Dynamical decoupling aims at modifying the system dynamics by applying sequences of control operations. A group theoretical framework underlies the method, and various strategies to design pulse sequences with high-level performance have been developed to suppress unwanted internal couplings and interactions with an environment.
6. To freeze the system evolution for long times, it is advantageous to merge together efficient deterministic sequences (such as the presented scheme leading to third-order decoupling) with randomized protocols. Randomization also proves useful in a time-varying system about which one has limited knowledge.
7. Although all protocols are essentially equivalent in the ideal limit of arbitrarily fast control, the outcome of sequences with finite intervals between controls is sensitive to the scheme selected, the final time considered, and the particularities of the system. Pulses insufficiently frequent may eventually lead to decoherence and tunneling acceleration.
8. Considering recent breakthroughs in active control methods based on electromagnetic pulses, we anticipate that the control scenarios reviewed in this article should raise significant experimental interest.

DISCLOSURE STATEMENT

The authors are not aware of any biases that might be perceived as affecting the objectivity of this review.

ACKNOWLEDGMENTS

L.G.C.R. gratefully acknowledges financial support from CNPq/Brazil. L.F.S. thanks Lorenza Viola for helpful discussions and start-up funds from Yeshiva University. V.S.B. acknowledges the NSF grants ECCS 0404191 and CHE 0345984, the DOE grant DE-FG02-07ER15909, and DOE supercomputer time from NERSC.

LITERATURE CITED

1. Devoret MH, Esteve D, Martinis JM, Cleland A, Clarke J. 1987. Resonant activation of a Brownian particle out of a potential well: microwave-enhanced escape from the zero-voltage state of a Josephson junction. *Phys. Rev. B* 36:58–73
2. Devoret MH, Estive D, Urbina C, Martinis J, Cleland A, Clarke J. 1992. *Quantum Tunneling in Condensed Media*. Amsterdam: North Holland
3. Martinis JM, Devoret MH, Clarke J. 1987. Experimental tests for the quantum behavior of a macroscopic degree of freedom: the phase difference across a Josephson junction. *Phys. Rev. B* 35:4682–98
4. **Rego LGC, Abuabara SG, Batista VS. 2005. Coherent optical control of electronic excitations in functionalized semiconductor nanostructures. *Quant. Inform. Comput.* 5:318–34**

4. Theoretical work demonstrating coherent optical control of superexchange hole tunneling in functionalized semiconductor nanostructures through sequences of phase-kick pulses.

5. **Rego LGC, Abuabara SG, Batista VS. 2006. Coherent control of tunneling dynamics in functionalized semiconductor nanostructures: a quantum-control scenario based on stochastic unitary pulses. *J. Mod. Opt.* 53:2519–32**
6. **Rego LGC, Abuabara SG, Batista VS. 2007. Multiple unitary pulses for coherent control of tunnelling and decoherence. *J. Mod. Opt.* 54:2617–27**
7. Dunlap DH, Kenkre VM. 1986. Dynamic localization of a charged particle moving under the influence of an electric field. *Phys. Rev. B* 34:3625–33
8. Grossmann F, Dittrich T, Jung P, Hanggi P. 1991. Coherent destruction of tunneling. *Phys. Rev. Lett.* 67:516–19
9. Facchi P, Pascazio S. 2002. Quantum Zeno subspaces. *Phys. Rev. Lett.* 89:080401
10. Itano WM, Heinzen DJ, Bollinger JJ, Wineland DJ. 1990. Quantum Zeno effect. *Phys. Rev. A* 41:2295–300
11. Koshino K, Shimizu A. 2005. Quantum Zeno effect by general measurements. *Phys. Rep.* 412:191–275
12. Pascazio S, Namiki M. 1994. Dynamical quantum Zeno effect. *Phys. Rev. A* 50:4582–92
13. Tasaki S, Tokuse A, Facchi P, Pascazio S. 2004. Control of decoherence: dynamical decoupling versus quantum Zeno effect—a case study for trapped ions. *Int. J. Quant. Chem.* 98:160–72
14. Peirce AP, Dahleh MA, Rabitz H. 1988. Optimal control of quantum-mechanical systems: existence, numerical approximation, and applications. *Phys. Rev. A* 37:4950–64
15. Rabitz H, de Vivie-Riedle R, Motzkus M, Kompa K. 2000. Chemistry: Whither the future of controlling quantum phenomena? *Science* 288:824–28
16. Carr HY, Purcell EM. 1954. Effects of diffusion on free precession in nuclear magnetic resonance experiments. *Phys. Rev.* 94:630–38
17. **Hahn EL. 1950. Spin echoes. *Phys. Rev.* 80:580–94**
18. Ernst RR, Bodenhausen G, Wokaun A. 1994. *Principles of Nuclear Magnetic Resonance in One and Two Dimensions*. Oxford: Oxford Univ. Press
19. Haeberlen U. 1976. *High Resolution NMR in Solids: Selective Averaging*. New York: Academic
20. Levitt MH. 2001. *Spin Dynamics: Basics of Nuclear Magnetic Resonance*. West Sussex, UK: Wiley & Sons
21. Waugh JS, Huber LM, Haeberle U. 1968. Approach to high-resolution NMR in solids. *Phys. Rev. Lett.* 20:180–92
22. Feynman RP, Vernon FL, Hellwarth RW. 1957. Geometrical representation of the Schrodinger equation for solving Maser problems. *J. Appl. Phys.* 28:49–52
23. Kurnit NA, Hartmann SR, Abella ID. 1964. Observation of photon echo. *Phys. Rev. Lett.* 13:567–73
24. Brumer P, Shapiro M. 1986. Control of unimolecular reactions using coherent light. *Chem. Phys. Lett.* 126:541–46
25. Brumer P, Shapiro M. 1989. Coherence chemistry: controlling chemical reactions with lasers. *Acc. Chem. Res.* 22:407–13
26. Shi SH, Woody A, Rabitz H. 1988. Optimal control of selective vibrational excitation in harmonic linear-chain molecules. *J. Chem. Phys.* 88:6870–83
27. Tannor DJ, Rice SA. 1985. Control of selectivity of chemical reaction via control of wave packet evolution. *J. Chem. Phys.* 83:5013–18
28. Tannor DJ, Rice SA. 1988. Coherent pulse sequence control of product formation in chemical reactions. *Adv. Chem. Phys.* 70:441–523
29. Batista VS, Brumer P. 2001. A direct approach to one photon interference contributions in the coherent control of photodissociation. *J. Chem. Phys.* 114:10321–31
30. Batista VS, Brumer P. 2001. Semiclassical dynamics in the coherent control of nonadiabatic ICN photodissociation. *J. Phys. Chem. A* 105:2591–98
31. Batista VS, Brumer P. 2002. Coherent control in the presence of intrinsic decoherence: proton transfer in large molecular systems. *Phys. Rev. Lett.* 89:143201
32. Batista VS, Brumer P. 2002. Erratum: coherent control in the presence of intrinsic decoherence: proton transfer in large molecular systems. *Phys. Rev. Lett.* 89:249903
33. Batista VS, Brumer P. 2003. Coherent control: principles and semiclassical implementations. In *Quantum Control: Mathematical and Numerical Challenges*, ed. A Bandrauk, C de Bris, pp. 59–78. Oxford: Oxford Univ. Press

5. Theoretical work demonstrating coherent optical control of tunneling based on stochastic sequences of phase-kick pulses.

6. Computer simulations demonstrating coherent control of bound-to-bound and bound-to-continuum tunneling in archetypical model systems and decoherence in quantum dots through multiple phase-kick pulses.

17. Experimental work demonstrating active control over coherent dynamics of molecular systems by the application of trains of RF π pulses.

34. Brumer P, Shapiro M. 1992. Laser control of molecular processes. *Annu. Rev. Phys. Chem.* 43:257–82
35. Brumer PW, Shapiro M. 2003. *Principles of the Quantum Control of Molecular Processes*. New York: Wiley & Sons
36. Chakrabarti R, Rabitz H. 2007. Quantum control landscapes. *Int. Rev. Phys. Chem.* 26:671–735
37. Flores SC, Batista VS. 2004. Model study of coherent control of the femtosecond primary event of vision. *J. Phys. Chem. B* 108:6745–49
38. Gordon RJ, Rice SA. 1997. Active control of the dynamics of atoms and molecules. *Annu. Rev. Phys. Chem.* 48:601–41
39. Rice SA, Zhao M. 2000. *Optical Control of Molecular Dynamics*. New York: Wiley & Sons
40. Warren WS, Rabitz H, Dahleh M. 1993. Coherent control of quantum dynamics: The dream is alive. *Science* 259:1581–89
41. Assion A, Baumert T, Bergt M, Brixner T, Kiefer B, et al. 1998. Control of chemical reactions by feedback-optimized phase-shaped femtosecond laser pulses. *Science* 282:919–22
42. Branderhorst MPA, Londero P, Wasylczyk P, Brif C, Kosut RL, et al. 2008. Coherent control of decoherence. *Science* 320:638–43
43. Brixner T, Damrauer NH, Niklaus P, Gerber G. 2001. Photoselective adaptive femtosecond quantum control in the liquid phase. *Nature* 414:57–60
44. Goswami D. 2003. Optical pulse shaping approaches to coherent control. *Phys. Rep.* 374:385–481
45. Becker PC, Fragnito HL, Bigot JY, Cruz CHB, Fork RL, Shank CV. 1989. Femtosecond photon echoes from molecules in solution. *Phys. Rev. Lett.* 63:505–7
46. Fragnito HL, Bigot JY, Becker PC, Shank CV. 1989. Evolution of the vibronic absorption spectrum in a molecule following impulsive excitation with a 6 fs optical pulse. *Chem. Phys. Lett.* 160:101–4
47. Mokhtari A, Chesnoy J, Laubereau A. 1989. Femtosecond time-resolved and frequency-resolved fluorescence spectroscopy of a dye molecule. *Chem. Phys. Lett.* 155:593–98
48. Gorman J, Hasko DG, Williams DA. 2005. Charge-qubit operation of an isolated double quantum dot. *Phys. Rev. Lett.* 95:090502
49. Hayashi T, Fujisawa T, Cheong HD, Jeong YH, Hirayama Y. 2003. Coherent manipulation of electronic states in a double quantum dot. *Phys. Rev. Lett.* 91:226804
50. Nakamura Y, Pashkin YA, Tsai JS. 1999. Coherent control of macroscopic quantum states in a single-Cooper-pair box. *Nature* 398:786–88
51. Turchette QA, Wood CS, King BE, Myatt CJ, Leibfried D, et al. 1998. Deterministic entanglement of two trapped ions. *Phys. Rev. Lett.* 81:3631–34
52. Preskill J. 1998. Reliable quantum computers. *Proc. R. Soc. Lond. Ser. A* 454:385–410
53. Steane AM. 1996. Error correcting codes in quantum theory. *Phys. Rev. Lett.* 77:793–97
54. Lidar DA, Chuang IL, Whaley KB. 1998. Decoherence-free subspaces for quantum computation. *Phys. Rev. Lett.* 81:2594–97
55. Viola L, Knill E, Lloyd S. 1999. Dynamical decoupling of open quantum systems. *Phys. Rev. Lett.* 82:2417–21
56. Viola L, Lloyd S. 1998. Dynamical suppression of decoherence in two-state quantum systems. *Phys. Rev. A* 58:2733–44
57. Viola L, Lloyd S, Knill E. 1999. Universal control of decoupled quantum systems. *Phys. Rev. Lett.* 83:4888–91
58. Zanardi P, Rasetti M. 1999. Holonomic quantum computation. *Phys. Lett. A* 264:94–99
59. Lapidus L, Luus R. 1967. *Optimal Control of Engineering Processes*. Waltham, MA: Blaisdell
60. Macki J, Strauss A. 1982. *Introduction to Optimal Control Theory*. New York: Springer-Verlag
61. Takahashi Y, Rabins MJ, Auslander DM. 1970. *Control and Dynamic Systems*. Reading, MA: Addison-Wesley
62. Santos LF. 2008. Transport control in low-dimensional spin-1/2 Heisenberg systems. *Phys. Rev. E* 78:031125
63. Shapiro EA, Walmsley IA, Vanov MY. 2007. Suppression of decoherence in a wave packet via nonlinear resonance. *Phys. Rev. Lett.* 98:050501
64. Vitali D, Tombesi P. 1999. Using parity kicks for decoherence control. *Phys. Rev. A* 59:4178–86

35. Presents the principles of the coherent optical control of molecular processes.

36. Demonstrates tailored pulses for optimal quantum control.

39. Optical control of molecular dynamics.

56. Theoretical work demonstrating suppression of decoherence in a two-level system through a sequence of π pulses.

65. Santos LF, Viola L. 2005. Dynamical control of qubit coherence: random versus deterministic schemes. *Phys. Rev. A* 72:062303
66. Santos LF, Viola L. 2008. Advantages of randomization in coherent quantum dynamical control. *New J. Phys.* In press
67. Viola L, Knill E. 2003. Robust dynamical decoupling of quantum systems with bounded controls. *Phys. Rev. Lett.* 90:037901
68. Khodjasteh K, Lidar DA. 2005. Fault-tolerant quantum dynamical decoupling. *Phys. Rev. Lett.* 95:180501
69. Khodjasteh K, Lidar DA. 2007. Performance of deterministic dynamical decoupling schemes: concatenated and periodic pulse sequences. *Phys. Rev. A* 75:062310
70. Jones JA, Knill E. 1999. Efficient refocusing of one-spin and two-spin interactions for NMR quantum computation. *J. Magn. Res.* 141:322–25
71. Stollsteimer M, Mahler G. 2001. Suppression of arbitrary internal coupling in a quantum register. *Phys. Rev. A* 64:052301
72. Uhrig GS. 2007. Keeping a quantum bit alive by optimized π-pulse sequences. *Phys. Rev. Lett.* 98: 100504
73. Falci G, D'Arrigo A, Mastellone A, Paladino E. 2004. Dynamical suppression of telegraph and 1/*f* noise due to quantum bistable fluctuators. *Phys. Rev. A* 70:040101
74. Faoro L, Viola L. 2004. Dynamical suppression of 1/*f* noise processes in qubit systems. *Phys. Rev. Lett.* 92:117905
75. Gutmann H, Wilhelm FK, Kaminsky WM, Lloyd S. 2005. Compensation of decoherence from telegraph noise by means of an open-loop quantum-control technique. *Phys. Rev. A* 71:020302
76. Shiokawa K, Lidar DA. 2004. Dynamical decoupling using slow pulses: efficient suppression of 1/*f* noise. *Phys. Rev. A* 69:030302
77. de Sousa R, Shenvi N, Whaley KB. 2005. Qubit coherence control in a nuclear spin bath. *Phys. Rev. B* 72:045310
78. Shenvi N, de Sousa R, Whaley KB. 2005. Universal scaling of hyperfine-induced electron spin echo decay. *Phys. Rev. B* 71:224411
79. Witzel WM, Das Sarma S. 2007. Concatenated dynamical decoupling in a solid-state spin bath. *Phys. Rev. B* 76:241303
80. Witzel WM, Das Sarma S. 2007. Multiple-pulse coherence enhancement of solid state spin qubits. *Phys. Rev. Lett.* 98:077601
81. Yao W, Liu RB, Sham LJ. 2007. Restoring coherence lost to a slow interacting mesoscopic spin bath. *Phys. Rev. Lett.* 98:077602
82. Zhang W, Konstantinidis NP, Dobrovitski VV, Harmon BN, Santos LF, Viola L. 2008. Long-time electron spin storage via dynamical suppression of hyperfine-induced decoherence in a quantum dot. *Phys. Rev. B* 77:125336
83. Zhang WX, Dobrovitski VV, Santos LF, Viola L, Harmon BN. 2007. Dynamical control of electron spin coherence in a quantum dot: a theoretical study. *Phys. Rev. B* 75:201302
84. Zhang WX, Dobrovitski VV, Santos LF, Viola L, Harmon BN. 2007. Suppression of electron spin decoherence in a quantum dot. *J. Mod. Opt.* 54:2629–40
85. Kern O, Alber G. 2005. Controlling quantum systems by embedded dynamical decoupling schemes. *Phys. Rev. Lett.* 95:250501
86. Kern O, Alber G. 2006. Selective recoupling and stochastic dynamical decoupling. *Phys. Rev. A* 73: 062302
87. Santos LF, Viola L. 2006. Enhanced convergence and robust performance of randomized dynamical decoupling. *Phys. Rev. Lett.* 97:150501
88. Viola L, Knill E. 2005. Random decoupling schemes for quantum dynamical control and error suppression. *Phys. Rev. Lett.* 94:060502
89. Viola L, Santos LF. 2006. Randomized dynamical decoupling techniques for coherent quantum control. *J. Mod. Opt.* 53:2559–68
90. Cory DG, Laflamme R, Knill E, Viola L, Havel TF, et al. 2000. NMR based quantum information processing: achievements and prospects. *Fortschr. Phys.* 48:875–907

87. Theoretical work demonstrating the advantages of randomization in coherent quantum dynamics.

91. Fraval E, Sellars MJ, Longdell JJ. 2005. Dynamic decoherence control of a solid-state nuclear-quadrupole qubit. *Phys. Rev. Lett.* 95:012332
92. Morton JJL, Tyryshkin AM, Ardavan A, Porfyrakis K, Lyon SA, Briggs GAD. 2005. Measuring errors in single-qubit rotations by pulsed electron paramagnetic resonance. *Phys. Rev. A* 71:012332
93. Nakamura Y, Pashkin YA, Yamamoto T, Tsai JS. 2002. Charge echo in a Cooper-pair box. *Phys. Rev. Lett.* 88:047901
94. Chiorescu I, Nakamura Y, Harmans C, Mooij JE. 2003. Coherent quantum dynamics of a superconducting flux qubit. *Science* 299:1869–71
95. Agarwal GS, Scully MO, Walther H. 2001. Accelerating decay by multiple 2π pulses. *Phys. Rev. A* 63:044101
96. Agarwal GS, Scully MO, Walther H. 2001. Inhibition of decoherence due to decay in a continuum. *Phys. Rev. Lett.* 86:4271–74
97. Wu LA, Lidar DA. 2002. Creating decoherence-free subspaces using strong and fast pulses. *Phys. Rev. Lett.* 88:207902
98. Matos-Abiague A, Berakdar J. 2004. Femtosecond control of electronic motion in semiconductor double quantum wells. *Phys. Rev. B* 69:155304
99. Matos-Abiague A, Berakdar J. 2004. Ultrafast control of electronic motion in quantum-well structures. *Appl. Phys. Lett.* 84:2346–48
100. Matos-Abiague A, Berakdar J. 2003. Controlling the orientation of polar molecules by half-cycle pulses. *Chem. Phys. Lett.* 382:475–80
101. Matos-Abiague A, Berakdar J. 2003. Sustainable orientation of polar molecules induced by half-cycle pulses. *Phys. Rev. A* 68:063411
102. Facchi P, Tasaki S, Pascazio S, Nakazato H, Tokuse A, Lidar DA. 2005. Control of decoherence: analysis and comparison of three different strategies. *Phys. Rev. A* 71:022302
103. Haroche S, Cohentan C, Audoin C, Scherman JP. 1970. Modified Zeeman hyperfine spectra observed in H-1 and Rb-87 ground states interacting with a nonresonant RF field. *Phys. Rev. Lett.* 24:861–67
104. Raab C, Eschner J, Bolle J, Oberst H, Schmidt-Kaler F, Blatt R. 2000. Motional sidebands and direct measurement of the cooling rate in the resonance fluorescence of a single trapped ion. *Phys. Rev. Lett.* 85:538–41
105. Keay BJ, Zeuner S, Allen SJ, Maranowski KD, Gossard AC, et al. 1995. Dynamic localization, absolute negative conductance, and stimulated, multiphoton emission in sequential resonant-tunneling semiconductor superlattices. *Phys. Rev. Lett.* 75:4102–5
106. Ivlev B. 2004. Tunneling through nonstationary barriers and Euclidean resonance. *Phys. Rev. A* 70:032110
107. Ivlev B. 2006. Tunneling in a magnetic field. *Phys. Rev. A* 73:052106
108. Ivlev B. 2007. Euclidean resonance in a magnetic field. *Phys. Rev. A* 76:022108
109. Ivlev B, Gudkov V. 2004. New enhanced tunneling in nuclear processes. *Phys. Rev. C* 69:037602
110. Ivlev B, Pepe G, Latempa R, Barone A, Barkov F, et al. 2005. Extreme multiphoton phenomena in Josephson junctions: Euclidean resonance. *Phys. Rev. B* 72:094507
111. Palomares-Baez JP, Ivlev B, Rodriguez-Lopez JL. 2007. Enhanced tunneling through nonstationary barriers. *Phys. Rev. A* 76:052103
112. Eckardt A, Weiss C, Holthaus M. 2005. Superfluid-insulator transition in a periodically driven optical lattice. *Phys. Rev. Lett.* 95:260404
113. Lignier H, Sias C, Ciampini D, Singh Y, Zenesini A, et al. 2007. Dynamical control of matter-wave tunneling in periodic potentials. *Phys. Rev. Lett.* 99:220403
114. Iyer R, Aitchison JS, Wan J, Dignam MM, de Sterke CM. 2007. Exact dynamic localization in curved AlGaAs optical waveguide arrays. *Opt. Expr.* 15:3212–23
115. Madison KW, Fischer MC, Diener RB, Niu Q, Raizen MG. 1998. Dynamical Bloch band suppression in an optical lattice. *Phys. Rev. Lett.* 81:5093–96
116. Della Valle G, Ornigotti M, Cianci E, Foglietti V, Laporta P, Longhi S. 2007. Visualization of coherent destruction of tunneling in an optical double well system. *Phys. Rev. Lett.* 98:263601
117. Longhi S, Marangoni M, Lobino M, Ramponi R, Laporta P, et al. 2006. Observation of dynamic localization in periodically curved waveguide arrays. *Phys. Rev. Lett.* 96:243901

96. Theoretical work demonstrating the inhibition of decoherence due to decay into a continuum through a sequence of unitary phase kick pulses.

118. Blick RH, Erbe A, Pescini L, Kraus A, Scheible DV, et al. 2002. Nanostructured silicon for studying fundamental aspects of nanomechanics. *J. Phys. Condens. Matter* 14:R905–45
119. Weig EM, Blick RH, Brandes T, Kirschbaum J, Wegscheider W, et al. 2004. Single-electron-phonon interaction in a suspended quantum dot phonon cavity. *Phys. Rev. Lett.* 92:046804
120. Gusso A, da Luz MGE, Rego LGC. 2006. Quantum chaos in nanoelectromechanical systems. *Phys. Rev. B* 73:035436
121. Rego LGC, Gusso A, da Luz MGE. 2005. Anomalous quantum chaotic behaviour in suspended electromechanical nanostructures. *J. Phys. A* 38:L639–45
122. Armour AD, Blencowe MP, Schwab KC. 2002. Entanglement and decoherence of a micromechanical resonator via coupling to a Cooper-pair box. *Phys. Rev. Lett.* 88:148301
123. Hohberger EM, Kramer T, Wegscheider W, Blick RH. 2003. In situ control of electron gas dimensionality in freely suspended semiconductor membranes. *Appl. Phys. Lett.* 82:4160–62
124. Beenakker CWJ. 1997. Random-matrix theory of quantum transport. *Rev. Mod. Phys.* 69:731–808
125. Hawrylak P. 1993. Single-electron capacitance spectroscopy of few-electron artificial atoms in a magnetic field: theory and experiment. *Phys. Rev. Lett.* 71:3347–50
126. Kouwenhoven LP, Austing DG, Tarucha S. 2001. Few-electron quantum dots. *Rep. Prog. Phys.* 64:701–36
127. Loss D, DiVincenzo DP. 1998. Quantum computation with quantum dots. *Phys. Rev. A* 57:120–26
128. Corso D, Pace C, Crupi F, Lombardo SA. 2007. Single-electron program/erase tunnel events in nanocrystal memories. *IEEE Trans. Nanotechnol.* 6:35–42
129. Abuabara SG, Cady CW, Baxter JB, Schmuttenmaer CA, Crabtree RH, et al. 2007. Ultrafast photooxidation of Mn(II)-terpyridine complexes covalently attached to TiO_2 nanoparticles. *J. Phys. Chem. C* 111:11982–90
130. Abuabara SG, Rego LGC, Batista VS. 2005. Influence of thermal fluctuations on interfacial electron transfer in functionalized TiO_2 semiconductors. *J. Am. Chem. Soc.* 127:18234–42
131. Rego LGC, Abuabara SG, Batista VS. 2005. Model study of coherent quantum dynamics of hole states in functionalized semiconductor nanostructures. *J. Chem. Phys.* 122:154079
132. Rego LGC, Batista VS. 2003. Quantum dynamics simulations of the interfacial electron transfer in sensitized TiO_2 semiconductors. *J. Am. Chem. Soc.* 125:7989–97
133. Nazeeruddin MK, Kay A, Rodicio I, Humphrybaker R, Muller E, et al. 1993. Conversion of light to electricity by Cis-X_2bis(2,2′-bipyridyl-4,4′-dicarboxylate)ruthenium(II) charge-transfer sensitizers (X = Cl-, Br-, I-, Cn-, and Scn-) on nanocrystalline TiO_2 electrodes. *J. Am. Chem. Soc.* 115:6382–90
134. O'Regan B, Gratzel M. 1991. A low-cost, high-efficiency solar cell based on dye-sensitized colloidal TiO_2 films. *Nature* 353:737–40
135. Duncan WR, Prezhdo OV. 2007. Theoretical studies of photoinduced electron transfer in dye-sensitized TiO_2. *Annu. Rev. Phys. Chem.* 58:143–84
136. Mills A, LeHunte S. 1997. An overview of semiconductor photocatalysis. *J. Photochem. Photobiol. A* 108:1–35
137. Serpone N. 1994. A decade of heterogeneous photocatalysis in our laboratory: pure and applied studies in energy production and environmental detoxification. *Res. Chem. Intermed.* 20:953–92
138. Serpone N, Lawless D, Disdier J, Herrmann JM. 1994. Spectroscopic, photoconductivity, and photocatalytic studies of TiO_2 colloids: naked and with the lattice doped with Cr^{3+}, Fe^{3+}, and V^{5+} cations. *Langmuir* 10:643–52
139. Serpone N, Terzian R, Hidaka H, Pelizzetti E. 1994. Ultrasonic induced dehalogenation and oxidation of 2-chlorophenol, 3-chlorophenol, and 4-chlorophenol in air-equilibrated aqueous media: similarities with irradiated semiconductor particulates. *J. Phys. Chem.* 98:2634–40
140. Levitt MH. 1982. Symmetrical composite pulse sequences for NMR population inversion. II. Compensation of resonance offset. *J. Magn. Reson.* 50:95–110
141. Levitt MH, Freeman R. 1981. Composite pulse decoupling. *J. Magn. Reson.* 43:502–7
142. Sengupta P, Pryadko LP. 2005. Scalable design of tailored soft pulses for coherent control. *Phys. Rev. Lett.* 95:037202
143. Slichter CP. 1992. *Principles of Magnetic Resonance*. Berlin: Springer-Verlag

144. Vandersypen LMK, Chuang IL. 2004. NMR techniques for quantum control and computation. *Rev. Mod. Phys.* 76:1037–69
145. Hess C. 2007. Heat conduction in low-dimensional quantum magnets. *Eur. Phys. J.* 151:73–83
146. Glazman LI, Larkin AI. 1997. New quantum phase in a one-dimensional Josephson array. *Phys. Rev. Lett.* 79:3736–39

Annual Review of
Physical Chemistry

Volume 60, 2009

Contents

Indexes

Errata

An online log of corrections to *Annual Review of Physical Chemistry* articles may be found at http://physchem.annualreviews.org/errata.shtml